Applied Catalysis B: Environment and Energy 350 (2024) 123926

Contents lists available at ScienceDirect

Applied Catalysis B: Environment and Energy

journal homepage: www.elsevier.com/locate/apcatb

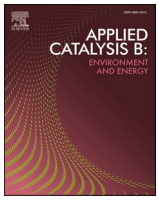

Enhanced Ru-O-Ce interaction by solid solution structure of Ru-$Ce_xZr_{1-x}O_2$ catalysts for efficient catalytic combustion of vinyl chloride

Baocheng Xie, Zijian Wei, Min Ding, Meixingzi Gao, Li Wang *, Wangcheng Zhan, Qiguang Dai, Yun Guo, Aiyong Wang *, Yanglong Guo *

State Key Laboratory of Green Chemical Engineering and Industrial Catalysis, Research Institute of Industrial Catalysis, School of Chemistry and Molecular Engineering, East China University of Science and Technology, Shanghai 200237, PR China

ARTICLE INFO

Keywords:
Catalytic combustion
CVOCs
Vinyl chloride
Ceria
Ru-O-Ce structure

ABSTRACT

Ru-$Ce_xZr_{1-x}O_2$ catalysts, prepared by stepwise precipitation method, were investigated for the catalytic combustion of vinyl chloride (VC). Ru-O-Ce is a highly reactive structure in the redox ability. The Ce-O-Zr solid solution structure enhances the strong metal-support-interaction (SMSI) between Ru and Ce, thereby increasing the content of Ru-O-Ce structure, which can be modulated by the molar ratio of Ce/(Ce + Zr) in the catalyst. Zr doping also enhances the surface acid sites. In situ DRIFTS reveals that Ru-$Ce_xZr_{1-x}O_2$ catalyst avoids chlorine poisoning, and Ru-O-Ce provides sufficient chemically adsorbed oxygen species (CAOS) to promote formation of formate intermediate species. Ru-$Ce_{0.5}Zr_{0.5}O_2$ catalyst exhibited the best catalytic performance with T_{90} of 227 °C under the reaction conditions of 1000 ppm VC and WHSV of 30,000 $mL \cdot g^{-1} \cdot h^{-1}$. Moreover, Ru-$Ce_{0.5}Zr_{0.5}O_2$ catalyst exhibited the superior resistance to high temperature, chlorine poisoning and water, and excellent catalytic activity for the catalytic combustion of various VOCs.

1. Introduction

Chlorine-containing chemicals are an important component of modern industrial manufacturing raw materials. Due to the limitation of technology, chlorinated volatile organic compounds (CVOCs) emissions are inevitably generated during the production chains. CVOCs emissions into the atmosphere are difficult to degrade naturally and can cause extremely serious hazards to the environment and human health [1–3]. There are several effective methods to eliminate CVOCs emissions in the industry, among which the catalytic combustion, with the advantages of lower reaction temperature, less secondary pollutions, and the ability to handle low concentrations of CVOCs, is regarded as a prosperous one [4,5]. Vinyl chloride (VC), as a kind of CVOCs, is widely employed in the production of polyvinyl chloride (PVC), which emits a large amount of low-concentration VC. Therefore, development of an efficient catalyst with excellent performance for the catalytic combustion of VC emission is an urgent challenge to be addressed.

Literatures reported various catalysts employed in the catalytic combustion of CVOCs, and the mainstream ones are transition-metal oxide catalysts, noble metal supported catalysts and zeolite catalysts. Among these catalysts, Ti, Mn, Co, Ce etc. as transition-metal oxide catalysts are readily available, relatively inexpensive and exhibit good redox performance, all of which have good catalytic activity [6–8]. The cyclic conversion of Ce^{3+} and Ce^{4+} on CeO_2 leads to a high content of surface oxygen vacancies and fast activation of O_2. That is why CeO_2 is mostly used as an oxygen-supply support or directly as an active component, but the poor dechlorination ability of CeO_2 results in deactivation, which is the main obstacle limiting its practical applications [9,10]. Noble metal supported catalysts (Pt, Pd, Rh) with high catalytic activity have been employed in the catalytic combustion of CVOCs, but such catalysts are prone to chlorine poisoning, resulting in high by-product selectivity and poor durability [11,12]. The noble metal of Ru has good resistance to chlorine poisoning, and can desorb the surface Cl species by forming Cl_2 through Deacon reaction, so there are various works on Ru/CeO_2 catalyst for the catalytic combustion of CVOCs [13,14]. However, it is difficult to effectively solve the issues of high selectivity to polychlorinated by-products and deactivation due to chlorine poisoning by only relying on Ru/CeO_2 catalyst, because Cl_2 is highly active and easy to form a variety of chlorinated by-products during the reaction process, and the complex chlorinated by-products further aggravate the problem of catalyst deactivation by chlorine poisoning.

* Corresponding authors.
E-mail addresses: wangli@ecust.edu.cn (L. Wang), wangaiyong@ecust.edu.cn (A. Wang), ylguo@ecust.edu.cn (Y. Guo).

https://doi.org/10.1016/j.apcatb.2024.123926
Received 18 December 2023; Received in revised form 11 February 2024; Accepted 6 March 2024
Available online 7 March 2024

Catalysts with better performance can be obtained through the modification of CeO_2 by doping other metal elements. For example, CeCr, CeTi, CeMn, CeSn have been reported for the catalytic combustion of CVOCs [6,15–17]. Our previous works indicate that the efficient catalytic oxidation of CVOCs requires both excellent redox properties and abundant surface acidic sites [7,18]. Zr-doped CeO_2 can simultaneously improve both the redox ability and the amount of surface acidic sites of the catalysts, and has been investigated in several catalytic oxidation reaction including CVOCs, showing a better catalytic activity than CeO_2 catalyst [19–22]. In the reported literatures, Ru-supported CeZr catalysts have been applied for catalytic wet air oxidation (CWAO) of 2-chlorophenol and succinic acid, but there is no relevant literature on its investigation into CVOCs [23,24]. In this work, we designed and successfully synthesized Ru-$Ce_xZr_{1-x}O_2$ catalysts with excellent catalytic performance, chlorine resistance, durability and water resistance for the catalytic combustion of VC emission. A series of characterizations revealed that by adjusting the content of Zr doping, the content of surface defects could be effectively regulated, thus increasing the amounts of highly reactive Ru-O-Ce structure, reactive oxygen species and surface acid sites. Moreover, reaction mechanism for the catalytic combustion of VC over Ru-$Ce_xZr_{1-x}O_2$ catalysts were proposed.

2. Experimental section

2.1. Catalyst synthesis

Ru-$Ce_xZr_{1-x}O_2$ catalysts with 0.5 wt% of Ru were synthesized by stepwise precipitation method. Took the synthesis of Ru-$Ce_{0.5}Zr_{0.5}O_2$ catalyst as an example and described it as follows. The deionized water (60 mL) was used to dissolve 2.21 g of $Ce(NO_3)_3$ and 1.57 g of $ZrO(NO_3)_2$. Then 0.38 g of 30 wt% of H_2O_2 was added dropwise based on the amount of $Ce(NO_3)_3$ and stirred for 30 min to ensure that Ce^{3+} was completely oxidized to Ce^{4+}. A certain amount of 28 wt% of $NH_3{\cdot}H_2O$ was added dropwise to adjust the solution pH value to 8–9 and stirred for 2 h. The resultant suspension was hydrothermally treated at 120 °C for 3 h. Then 0.15 g of $RuCl_3$ solution (Ru content of 0.67 wt%) was added dropwise into the hydrothermally treated suspension at 55 °C and stirred for 3 h. The dark gray product was washed, dried at 60 °C overnight and then calcined at 500 °C for 4 h. Other catalysts were also synthesized by the above method using different amounts of precursors. The obtained catalysts were designated as Ru-$Ce_xZr_{1-x}O_2$, in which x was the molar ratio of Ce/(Ce + Zr).

2.2. Activity evaluation

The catalytic combustion of VC was carried out in the quartz fixed-bed reactor with 6 mm inner diameter. The catalyst (0.24 g, 40–60 meshes) was investigated under the reaction conditions of 1000 ppm VC and the balanced air, and weight hourly space velocity (WHSV) of 30,000 $mL{\cdot}g^{-1}{\cdot}h^{-1}$. To eliminate the effects of ex-internal diffusions, the height of catalyst bed was set at 25 mm with quartz sands of 40–60 meshes. The reaction products were analyzed with an online gas chromatography with a flame ionization detector (FID) and a SE-30 capillary column of 50 m*0.53 mm*1.0 μm. VC conversion was calculated by the difference in VC concentrations before and after the fixed-bed reactor. VC concentration after the reactor was determined after reaction for 40 min at a specified reaction temperature.

2.3. Catalyst characterization

The physicochemical properties of $Ce_xZr_{1-x}O_2$ catalysts were characterized by powder X-ray diffraction (XRD), N_2 sorption, Raman spectrometer, X-ray photoelectron spectroscopy (XPS), ICP-AES, temperature-programed reduction of H_2 (H_2-TPR), temperature-programed desorption of O_2 (O_2-TPD) and CO pulse adsorption. The amount and type of acid sites on the catalyst surface were obtained by temperature-programed desorption of NH_3 (NH_3-TPD) and in situ DRIFTS for NH_3 adsorption at 100 °C. The intermediate species in the catalytic combustion of VC were characterized by in situ DRIFTS for VC and O_2 adsorption at different temperatures. The detailed characterization process was given in the supporting information.

3. Results and discussion

3.1. XRD and Raman

XRD patterns of Ru-$Ce_xZr_{1-x}O_2$ catalysts are shown in Fig. 1a. There were two kinds of main diffraction peaks for Ru-$Ce_xZr_{1-x}O_2$ catalysts. Ru-$Ce_xZr_{1-x}O_2$ catalysts ($x \geq 0.3$) exhibited the diffraction peaks at 2θ = 28.5°, 33.0°, 47.5°, 56.3°, which represented the cubic phase of CeO_2 (in accordance with JCPDS NO.43–1002). When x = 0.1, the crystalline phase of Ru-$Ce_xZr_{1-x}O_2$ catalyst changed to the tetragonal phase of ZrO_2 (JCPDS NO.49–1642) with the diffraction peaks at 2θ = 30.1°, 34.9°, 50.3°, 59.8°. As for Ru-ZrO_2 catalyst, it was consisted with the tetragonal and monoclinic phases of ZrO_2. With an increase in Zr doping ratio, the diffraction peaks gradually shifted to higher angles and the diffraction peaks got broader for Ru-$Ce_xZr_{1-x}O_2$ catalysts ($x \geq 0.3$). The shift of diffraction peaks was caused by the different ionic radius between Zr^{4+} (0.84 Å) and Ce^{4+} (0.97 Å), when Ce^{4+} was partly replaced by Zr^{4+} with smaller ionic radius, a Ce-O-Zr solid solution was formed along with lattice distortion [25], which was confirmed by the decrease of lattice parameters of Ru-$Ce_xZr_{1-x}O_2$ catalysts shown in Table 1 with increasing Zr doping ratio. The broadening of diffraction peaks was caused by the degradation of crystallinity due to solid solution structure. When Zr doping ratio reached 0.9, the tetragonal phase of ZrO_2 became a dominant crystalline phase. The absence of diffraction peaks of monoclinic phase of ZrO_2 was because the cubic structure of CeO_2 was similar to that of the tetragonal ZrO_2, which was beneficial to form a tetragonal solid solution structure. Moreover, no characteristic diffraction peaks of Ru species were observed due to low Ru contents or good dispersion of Ru species on the catalyst surface [26].

The physicochemical properties of Ru-$Ce_xZr_{1-x}O_2$ catalysts are summarized in Table 1. As shown in Table 1, the crystallite diameter, specific surface area and Ru dispersion of Ru-$Ce_xZr_{1-x}O_2$ catalysts showed a volcano-like curve, indicating that these physicochemical parameters were affected by the molar ratio of Ce/(Ce + Zr) of Ru-$Ce_xZr_{1-x}O_2$ catalysts. Among these catalysts, Ru-$Ce_{0.5}Zr_{0.5}O_2$ catalyst had the smallest crystallite diameter, the largest specific surface area and the optimal Ru dispersion, corresponding to 4.9 nm, 130 $m^2{\cdot}g^{-1}$, 69%, respectively. The generation of solid solution structure leads to formation of surface defects [21,22]. High defect content is beneficial to generate high specific surface area, which is conducive to VC adsorption on the catalyst surface. The actual Ru contents of Ru-$Ce_xZr_{1-x}O_2$ catalysts, measured by ICP-AES, were close to the feed Ru contents of 0.5 wt%, which indicated that Ru was mostly supported on the catalyst surface. Higher Ru dispersion indicated a stronger interaction between Ru and $Ce_xZr_{1-x}O_2$ support, which was strengthened by Zr doping into Ru-CeO_2 according to the results of Ru dispersion shown in Table 1, thus optimizing the catalytic performance of the resultant catalyst.

Raman spectra of Ru-$Ce_xZr_{1-x}O_2$ catalysts are shown in Fig. 1b. For Ru-$Ce_{0.1}Zr_{0.9}O_2$ and Ru-ZrO_2 (Fig. 1b(II)) catalysts, the bands at 145, 268, 330, 474 and 636 cm^{-1} were attributed to the tetragonal ZrO_2, and the bands at 187, 377 and 615 cm^{-1} were assigned to the monoclinic ZrO_2 [22,27]. After introduction of Ce into ZrO_2 structure, the monoclinic structure disappeared, which was consistent with XRD results. As for Ru-$Ce_xZr_{1-x}O_2$ ($x \geq 0.3$) catalysts shown in Fig. 1b(I), the band at 460 cm^{-1} was attributed to the symmetrical stretching F_{2g} mode of Ce-O [28]. Three bands at 258, 597 and 1172 cm^{-1} were assigned to second-order transverse acoustic (2TA) mode, defect-induced (D) mode, and second-order longitudinal optical (2LO) mode, respectively [29]. The bands at 691 and 970 cm^{-1} were assigned to Ru-O-Ce bond [30].

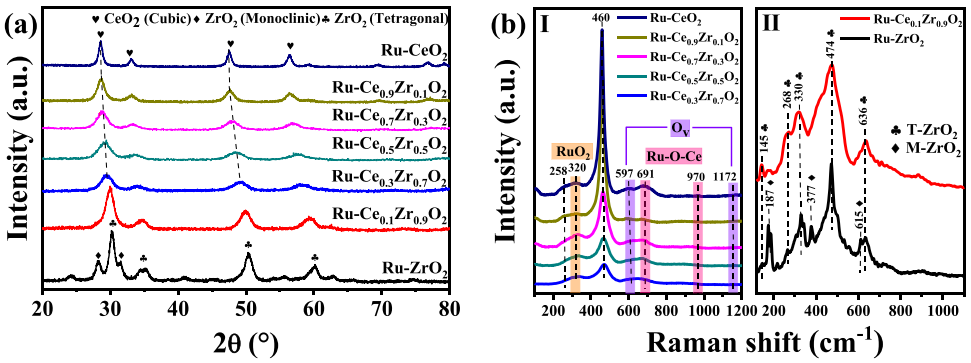

Fig. 1. (a) XRD patterns of Ru-$Ce_xZr_{1-x}O_2$ catalysts, (b) Raman spectra of (I) Ru-$Ce_xZr_{1-x}O_2$, (II) Ru-$Ce_{0.1}Zr_{0.9}O_2$ and Ru-ZrO_2 catalysts.

Table 1
Physicochemical properties of Ru-$Ce_xZr_{1-x}O_2$ catalysts.

Samples	2θ (°)	Lattice parameter[a] (Å)	D[b] (nm)	S_{BET} ($m^2 \cdot g^{-1}$)	Ru content[c] (wt%)	Ru dispersion[d] (%)
Ru-ZrO_2	30.23	5.11	9.6	91	0.50	44
Ru-$Ce_{0.1}Zr_{0.9}O_2$	29.95	5.16	5.7	99	0.54	39
Ru-$Ce_{0.3}Zr_{0.7}O_2$	29.48	5.31	5.1	128	0.51	61
Ru-$Ce_{0.5}Zr_{0.5}O_2$	29.15	5.33	4.9	130	0.48	69
Ru-$Ce_{0.7}Zr_{0.3}O_2$	28.68	5.38	5.2	118	0.49	62
Ru-$Ce_{0.9}Zr_{0.1}O_2$	28.63	5.40	6.6	74	0.48	63
Ru-CeO_2	28.54	5.41	8.9	43	0.47	32

[a] Calculated by (111) facet from XRD patterns
[b] Calculated by Scherrer equation from XRD patterns
[c] Measured by ICP-AES
[d] Measured by CO pulse adsorption

The band at 320 cm^{-1} was assigned to vibration of RuO_2 species [14]. The replacement of Ce^{4+} by Zr^{4+} reduced the mean length of M-O bond, leading to a blue shift of the band at 460 cm^{-1}. This result was consistent with the shift of diffraction peak in XRD pattern (Fig. 1a) and the decrease of lattice parameter determined by XRD pattern (Table 1) [31, 32]. This blue shift proved the existence of Ce-O-Zr solid solution structure. The bandwidth of Ru-$Ce_xZr_{1-x}O_2$ catalysts was significantly wider than that of Ru-CeO_2 catalyst, which also confirmed the formation of solid solution structure.

According to Raman analysis, the intensity ratio of $I_{(597+1172)}/I_{460}$ represented the concentration of oxygen vacancies, and the intensity ratio of $I_{(691+970)}/I_{460}$ represented the concentration of Ru-O-Ce bond of Ru-$Ce_xZr_{1-x}O_2$ catalysts with cubic fluorite structure [29]. The calculated values of both $I_{(597+1172)}/I_{460}$ and $I_{(691+970)}/I_{460}$ are summarized in Table 2. The molar ratio of Ce/(Ce + Zr) greatly affected the surface properties of $Ce_xZr_{1-x}O_2$ supports, which influenced the binding state of Ru on the support surface. Ru-$Ce_{0.5}Zr_{0.5}O_2$ catalyst exhibited the highest $I_{(597+1172)}/I_{460}$ value of 0.253. In general, the more defects there are, the higher concentration of oxygen vacancies there is. According to the above results, the solid solution structure was beneficial for generating surface defects. Therefore, when Ce-O-Zr solid solution structure with Ce/(Ce + Zr) of 0.5 was formed, the most surface defects were generated. Moreover, Ru was adsorbed on the surface defect sites and then interacted with Ce to generate Ru-O-Ce bond. High defect concentration favored an increase in Ru dispersion and the concentration of Ru-O-Ce bond. The same variation trends existed between $I_{(691+970)}/I_{460}$ ratio of Ru-O-Ce bond concentration and $I_{(597+1172)}/I_{460}$ ratio of the oxygen vacancy concentration. Ru-$Ce_{0.5}Zr_{0.5}O_2$ catalyst also had the highest $I_{(691+970)}/I_{460}$ value of 0.282.

Table 2
Surface compositions of Ru-$Ce_xZr_{1-x}O_2$ catalysts.

Samples	Raman spectra		Ce^{3+}/Ce	O_{ad}/O_L	Ru^{n+}/Ru
	$I_{(597+1172)}/I_{460}$	$I_{(691+970)}/I_{460}$			
Ru-ZrO_2	/	/	/	0.287	/
Ru-$Ce_{0.1}Zr_{0.9}O_2$	/	/	0.267	0.307	0.50
Ru-$Ce_{0.3}Zr_{0.7}O_2$	0.248	0.246	0.279	0.341	0.51
Ru-$Ce_{0.5}Zr_{0.5}O_2$	0.253	0.282	0.282	0.421	0.54
Ru-$Ce_{0.7}Zr_{0.3}O_2$	0.139	0.147	0.209	0.272	0.50
Ru-$Ce_{0.9}Zr_{0.1}O_2$	0.051	0.036	0.197	0.254	0.40
Ru-CeO_2	0.064	0.073	0.199	0.263	0.48

3.2. XPS

Fig. 2 shows Ce 3d, O 1 s and Ru 3d XPS spectra of Ru-$Ce_xZr_{1-x}O_2$ catalysts. As shown in Fig. 2a, Ce 3d spectra were fitted with ten peaks according to five pairs of spin-orbit doublets [33]. The peaks labeled as ν (882.4 eV), ν'' (888.8 eV) and ν''' (898.1 eV) were assigned to Ce^{4+} $3d_{5/2}$. The peaks labeled as u (901.8 eV), u'' (907.2 eV) and u''' (916.5 eV) were assigned to Ce^{4+} $3d_{3/2}$. Another four peaks labeled as ν_0 (882.3 eV), ν' (885.5 eV), and u_0 (900.7 eV), u' (903.9 eV) were assigned to Ce^{3+} $3d_{5/2}$ and Ce^{3+} $3d_{3/2}$, respectively. As shown in Table 2, the molar ratio of Ce/(Ce + Zr) greatly influenced Ce^{3+} content, and the values of Ce^{3+}/Ce of Ru-$Ce_xZr_{1-x}O_2$ catalysts (x = 0.1, 0.3, 0.5, 0.7, 0.9, 1) were 0.267, 0.279, 0.282, 0.209, 0.197, 0.199, respectively. It is known that the formation of Ce^{3+} is beneficial to create the surface oxygen vacancies [34]. The content of Ce^{3+} as a function of the molar ratio of Ce/(Ce + Zr) exhibited a volcano-like trend, which was consistent with Raman-derived trend of the concentration of oxygen vacancies (Figure S1). According to XRD and Raman results, doping of Zr formed the solid solution structure, which could increase the concentration of surface defects and the concentration of Ru-O-Ce bond. Combined with the results of Ce 3d XPS spectra, Ru-O-Ce structure on

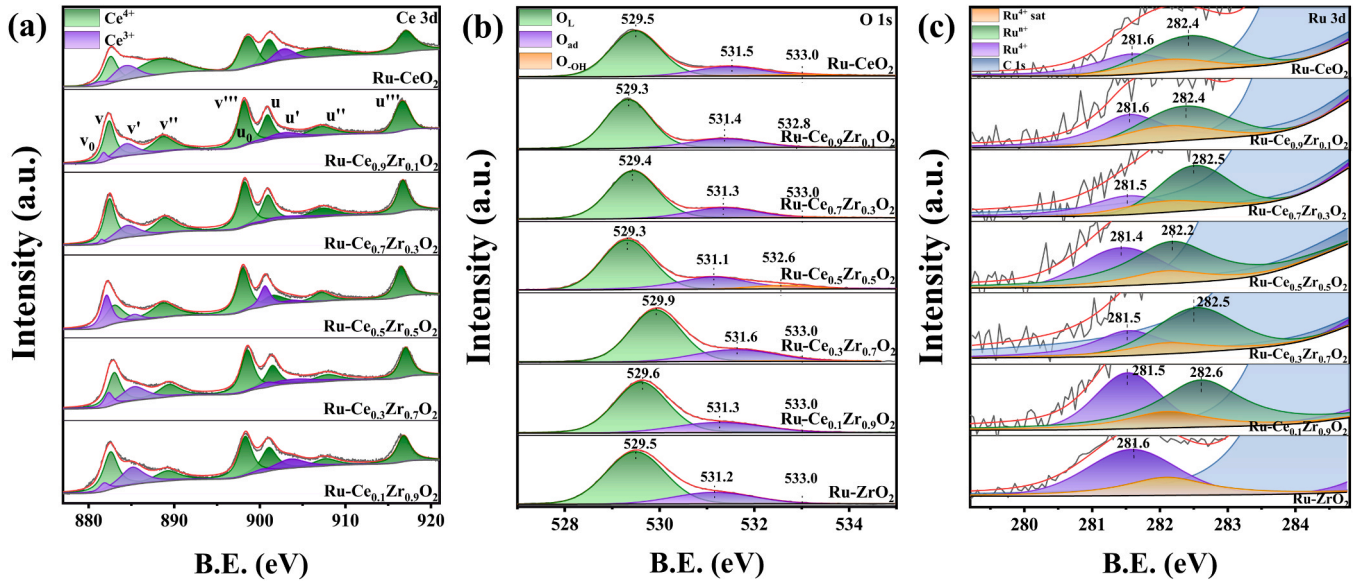

Fig. 2. (a) Ce 3d, (b) O 1 s and (c) Ru 3d XPS spectra of Ru-$Ce_xZr_{1-x}O_2$ catalysts.

the catalyst surface facilitated conversion of Ce^{4+} to Ce^{3+}.

O 1 s XPS spectra of Ru-$Ce_xZr_{1-x}O_2$ catalysts, shown in Fig. 2b, were deconvoluted into three peaks at 529.3–529.9 eV, 531.1–531.6 eV, 532.5–533.0 eV, which were assigned to lattice oxygen species (labeled as O_L), surface chemically adsorbed oxygen species (labeled as O_{ad}) and other oxygen species such as -OH (labeled as O_{-OH}), respectively [18,35]. Oxygen in the air was adsorbed on the oxygen vacancy and activated as a chemically adsorbed oxygen species. As mentioned above, Ce^{3+} facilitated the generation of oxygen vacancies, so the content of chemisorbed oxygen species was positively correlated with Ce^{3+} content. Among all oxygen species, O_{ad} species played an essential role in the catalytic combustion of VC [36,37]. As summarized in Table 2, the values of O_{ad} / O_L were 0.287, 0.307, 0.341, 0.421, 0.272, 0.254 and 0.263 over Ru-$Ce_xZr_{1-x}O_2$ catalysts (x = 0, 0.1, 0.3, 0.5, 0.7, 0.9, 1), respectively. The change trend of O_{ad} / O_L values matched that of Ce^{3+}/Ce.

Ru 3d XPS spectra of Ru-$Ce_xZr_{1-x}O_2$ catalysts are shown in Fig. 2c. The deconvoluted peaks at ~281.5 eV were attributed to Ru^{4+}, with the corresponding satellite peaks at ~282.1 eV [38–40]. The peaks at 282.2–282.6 eV were assigned to $Ru^{n+\ (4<n<6)}$ of Ru-O-Ce bond [41]. The valence states of Ru on the catalyst surface were influenced by the interfacial charge transfer between RuO_x and $Ce_xZr_{1-x}O_2$ support, and the extent of charge transfer was dependent on the strength of strong metal-support interaction (SMSI) [42]. Raman spectra (Fig. 1b) indicated presence of Ru-O-Ce bond, therefore Ru^{n+} was caused by electron transfer between RuO_2 and the solid solution support in the form of Ru-O-Ce bond. There was no Ru^{n+} peak in Ru 3d XPS spectra of Ru-ZrO_2 catalyst, which also confirmed that the element interaction with Ru was Ce rather than Zr. After fitting the peaks of Ru 3d spectra, Ru^{n+}/Ru is summarized in Table 2. As seen in Table 2, the change trend of Ru^{n+}/Ru value was consistent with the concentration variation of Ru-O-Ce bond calculated from Raman results (Figure S2). The electron transfer in the form of Ru-O-Ce bond further increased Ce^{3+} content on the catalyst surface.

As shown in Figure S3, Zr 3d XPS spectra of Ru-ZrO_2 catalyst exhibited two peaks at 181.6 and 184.0 eV assigned to Zr $3d_{3/2}$ and $3d_{5/2}$, respectively. The Zr^{4+} binding energy of Ru-$Ce_xZr_{1-x}O_2$ catalysts was higher than that of Ru-ZrO_2 catalyst, which was caused by the entrance of Zr^{4+} into CeO_2 lattice forming Ce-O-Zr solid solution structure [22]. In addition, the Zr^{4+} binding energy of Ru-$Ce_xZr_{1-x}O_2$ catalysts ($0.3 \leq x \leq 0.9$) was almost identical but higher than that of Ru-$Ce_{0.1}Zr_{0.9}O_2$ catalyst, indicating that the binding energy of Zr^{4+} was affected by the catalyst structure, and the trend of which was consistent with XRD and Raman results.

3.3. Redox property of catalysts

Fig. 3 shows H_2-TPR and O_2-TPD profiles of Ru-$Ce_xZr_{1-x}O_2$ catalysts. As shown in Fig. 3a, for Ru-CeO_2 and Ru-ZrO_2 catalysts, the actual H_2 consumption at low temperature (labeled as α in Table 3) was much higher than the theoretical H_2 consumption of RuO_2 (0.099 mmol·g^{-1}). Therefore, the reduction peaks at low temperature (109 °C and 91 °C, respectively) were attributed to reduction of surface highly dispersed RuO_2 species and adsorbed oxygen species [29,43]. As for solid solution structure of Ru-$Ce_xZr_{1-x}O_2$ catalysts, there were two different reduction peaks in low temperature range of 90–121 °C, indicating that Ru species existed in two different states on the catalyst surface. The reduction peaks at relatively low temperature were attributed to reduction of surface highly dispersed RuO_2 species and adsorbed oxygen species. The reduction peaks at relatively high temperature were probably assigned to reduction of surface oxygen species of support around Ru (Ru-O-Ce) [42,44,45]. As shown in Figure S4, the reduction peak at low temperature of Ru-CeO_2 catalyst was fitted and exhibited two reduction peaks at 106 and 120 °C, respectively, which was consistent with other Ru-$Ce_xZr_{1-x}O_2$ catalysts. The intensity and reduction temperature of these two peaks were greatly influenced by the molar ratio of Ce/(Ce + Zr). Compared with Ru-ZrO_2 catalyst, the appearance of new reduction peak proved existence of Ru-O-Ce structure and surface defects, in accordance with the above Raman and XPS results, which was helpful to form this structure on the catalyst surface. The reduction peaks at higher temperature were assigned to reduction of surface lattice oxygen species, with the reduction temperature at 368 °C and 330 °C for Ru-CeO_2 and Ru-ZrO_2 catalysts, respectively. With increasing Ru-O-Ce concentration caused by the solid solution structure, the reduction temperature decreased to 298 °C, 293 °C, 306 °C, 329 °C and 352 °C for Ru-$Ce_xZr_{1-x}O_2$ catalysts (x = 0.1, 0.3, 0.5, 0.7, 0.9), respectively. Lower reduction temperature meant more reactive oxygen species. H_2 consumption of lattice oxygen species also increased (labeled as β in Table 3) with decreasing reduction temperature, indicating a significant increase in the number of oxygen species. Among Ru-$Ce_xZr_{1-x}O_2$ catalysts, Ru-$Ce_{0.3}Zr_{0.7}O_2$ catalyst exhibited lower O_L reduction temperature compared with Ru-$Ce_{0.5}Zr_{0.5}O_2$ catalyst, but H_2 consumption of Ru-$Ce_{0.3}Zr_{0.7}O_2$ catalyst (1.49 mmol·g^{-1}) was much lower than that of Ru-$Ce_{0.5}Zr_{0.5}O_2$ catalyst (2.22 mmol·g^{-1}). O_L was mainly involved in oxygen cycling at high temperature, thus the amount of which was more

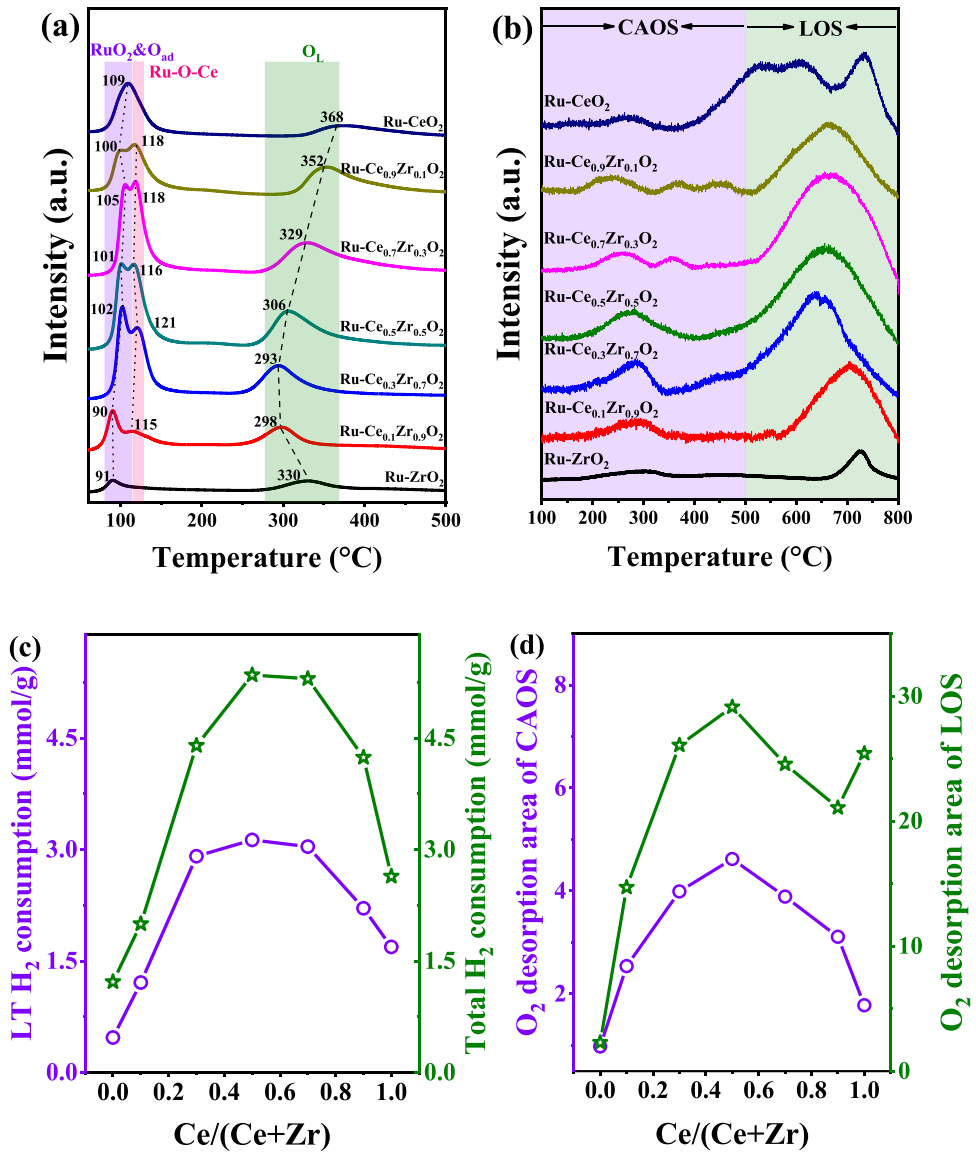

Fig. 3. (a) H_2-TPR, (b) O_2-TPD profiles, (c) change trend of LT and total H_2 consumption and (d) contents of CAOS and LOS of Ru-$Ce_xZr_{1-x}O_2$ catalysts.

Table 3
H_2 consumption and contents of oxygen species of Ru-$Ce_xZr_{1-x}O_2$ catalysts.

Samples	H_2 consumption (mmol·g^{-1})			Content of oxygen species (a.u.)	
	α (T/°C)	β (T/°C)	total	Area of CAOS	Area of LOS
Ru-ZrO_2	0.47 (91)	0.75 (330)	1.22	1.00[a]	2.34
Ru-$Ce_{0.1}Zr_{0.9}O_2$	1.21 (90)	0.79 (298)	2.00	2.59	15.00
Ru-$Ce_{0.3}Zr_{0.7}O_2$	2.91 (102)	1.49 (293)	4.40	4.07	26.60
Ru-$Ce_{0.5}Zr_{0.5}O_2$	3.13 (101)	2.22 (306)	5.35	4.71	29.71
Ru-$Ce_{0.7}Zr_{0.3}O_2$	3.04 (105)	2.26 (329)	5.30	3.97	25.05
Ru-$Ce_{0.9}Zr_{0.1}O_2$	2.21 (100)	2.03 (352)	4.24	3.17	21.50
Ru-CeO_2	1.69 (109)	0.95 (368)	2.64	1.82	25.93

[a] This fitted peak area was used for normalization.

important when the reduction temperature did not differ much.

The consumption amounts of H_2 at different reduction temperatures are summarized in Table 3. According to the total consumption amount of H_2, the promotion of Ru-O-Ce bonds on the catalyst surface by solid solution structure greatly increased the redox ability of Ru-$Ce_xZr_{1-x}O_2$ catalysts. Taking Ru-CeO_2 and Ru-$Ce_{0.5}Zr_{0.5}O_2$ catalysts as examples, the molar ratio of Zr doping of 0.5 increased the redox ability by twice (2.64 and 5.35 mmol·g^{-1}, respectively). To further confirm contribution of Ru-O-Ce bonds to the redox ability of catalysts, H_2-TPR experiment was used to characterize $Ce_xZr_{1-x}O_2$ supports shown in Figure S5. No reduction peaks at the reduction temperature lower than 400 °C were observed, which proved the promotion effect of Ru-O-Ce bonds. According to the consumption amount of H_2 shown in Table 3 and Table S1, the solid solution structure greatly increased the number of oxygen species on the catalyst surface. For $Ce_{0.5}Zr_{0.5}O_2$ sample, the consumption amount of H_2 was 1.378 mmol·g^{-1}, much higher than that of CeO_2 sample of 0.509 mmol·g^{-1}. Especially, a low-temperature reduction peak at 457 °C appeared over $Ce_{0.5}Zr_{0.5}O_2$ sample, indicating that partial Ce^{4+} species was easily reduced. This result also confirmed that the optimal molar ratio of Ce/(Ce + Zr) was 0.5. Another point worth noting was the difference in the reduction temperatures

between Ru-$Ce_xZr_{1-x}O_2$ catalysts and Ru-free samples. As shown in Figure S5, for Ru-free samples, the reduction temperature shifted to higher temperature after formation of Ce-O-Zr solid solution structure, which indicated that the main benefit of solid solution structure was to increase the amount of oxygen species rather than activate surface oxygen species. The change trend of reduction temperature of lattice oxygen species of $Ce_xZr_{1-x}O_2$ samples was quite different from that of Ru-$Ce_xZr_{1-x}O_2$ catalysts, in which the reduction temperature of Ru-$Ce_xZr_{1-x}O_2$ catalysts shifted to lower temperature after formation of solid solution structure. Taking the change distinction of reduction temperature between Ru-CeO_2, CeO_2 and Ru-$Ce_{0.5}Zr_{0.5}O_2$, $Ce_{0.5}Zr_{0.5}O_2$ catalysts as examples, the reduction temperature decreased from 535 °C of CeO_2 to 368 °C of Ru-CeO_2, whereas in the samples with solid solution structure, the reduction temperature decreased from 569 °C of $Ce_{0.5}Zr_{0.5}O_2$ to 306 °C of Ru-$Ce_{0.5}Zr_{0.5}O_2$, the decrease in the reduction temperature was much larger than the former one. This difference proved the important role of the solid solution structure in formation of Ru-O-Ce bonds to improve the redox ability of Ru-$Ce_xZr_{1-x}O_2$ catalysts.

O_2-TPD profiles of Ru-$Ce_xZr_{1-x}O_2$ catalysts are shown in Fig. 3b. As shown in Fig. 3b, there were two kinds of desorption peaks. The desorption peaks below 500 °C were assigned to chemically adsorbed oxygen species (CAOS), which was the primary oxygen species involved in the catalytic combustion reaction, and the desorption peaks above 500 °C were assigned to lattice oxygen species (LOS) [18,46]. For Ru-CeO_2 and Ru-ZrO_2 catalysts, the intensities of desorption peaks of CAOS were weak. The intensity of desorption peak of CAOS significantly increased and the desorption temperature also decreased after formation of the solid solution structure. Three kinds of lattice oxygen species were observed over Ru-CeO_2 catalyst and the two desorption peaks with lower temperatures were assigned to the lattice oxygen species closing to the surface RuO_2 (Ru-O-Ce), which were not observed over Ru-ZrO_2 catalyst. When Zr was doped into CeO_2 lattice to form Ce-O-Zr solid solution structure, such as Ru-$Ce_{0.9}Zr_{0.1}O_2$ catalyst shown in Fig. 3b, these two desorption peaks shifted to lower temperature and became chemically adsorbed oxygen species, indicating that higher content of Ru-O-Ce bond, enhanced by the solid solution structure, was beneficial to further activate lattice oxygen species and enhance their mobility. With an increase in Zr doping ratio, the desorption peaks continuously shifted to lower temperature and eventually fused with the initial low temperature peak (~275 °C) of Ru-CeO_2 catalyst. Additionally, the third desorption peak of LOS also shifted to lower temperature and the peak area increased. The activation of partial LOS into CAOS and the increase in the area of desorption peaks confirmed the promotional effect of the solid solution structure on the content of Ru-O-Ce bond to enhance the redox ability. The desorption peak from activation of partial LOS, generated by Ru-O-Ce bond, had a desorption temperature higher than that of CAOS, which also matched the two low-temperature reduction peaks in H_2-TPR profiles. The LOS of Ru-$Ce_{0.3}Zr_{0.7}O_2$ catalyst exhibited lower desorption temperature but smaller desorption area compared with that of Ru-$Ce_{0.5}Zr_{0.5}O_2$ catalyst, which was consistent with the O_L result of H_2-TPR profiles. The change trend of the desorption peak areas shown in Fig. 3d was similar to that of H_2-TPR shown in Fig. 3c. Therefore Ru-O-Ce bond could activate partial lattice oxygen species to form chemically adsorbed oxygen species and enhance the surface oxygen species of Ru-$Ce_xZr_{1-x}O_2$ catalysts with excellent redox ability. Doping of Zr into CeO_2 lattice to form Ce-O-Zr solid solution structure is an effective way to increase Ru-O-Ce content on the catalyst surface.

3.4. Surface acidity of catalysts

NH_3-TPD profiles of Ru-$Ce_xZr_{1-x}O_2$ catalysts are shown in Fig. 4a. ZrO_2, as a solid acid, is frequently added to other metal oxides to improve the surface acidity [47]. With an increase in Zr doping ratio, the intensity of desorption peak increased gradually. The broad desorption peaks were deconvoluted into three different kinds of acid sites (labeled as α, β and γ), which were attributed to weak acid sites (lower than 200 °C), medium acid sites (200–300 °C) and strong acid sites (300–400 °C), respectively [7,18]. The amount of acid sites is summarized in Table S2. As shown in Table S2, the main acid sites of Ru-CeO_2 were medium acid sites and those of Ru-ZrO_2 were strong acid sites. The change trend of the content of different acid sites vs. the molar ratio of Ce/(Ce + Zr) is shown in Fig. 4c. For Ru-$Ce_xZr_{1-x}O_2$ catalysts ($0.1 \leq x \leq 0.9$) with solid solution structure, medium and strong acid sites increased with increasing Zr doping ratio. As shown in Table S2, the total acid sites also increased with an increase in Zr doping ratio.

In situ DRIFTS of NH_3 at 100 °C over Ru-$Ce_xZr_{1-x}O_2$ catalysts are shown in Fig. 4b, in which the adsorption bands at 1350, 1406 and 1550 cm^{-1} were attributed to Brønsted acid sites [49], while the adsorption bands at 1078, 1144, 1180, 1276 and 1578 cm^{-1} were attributed to Lewis acid sites [48,49]. For Ru-CeO_2 catalyst, there were a comparable amounts of Lewis acid and Brønsted acid sites. Compared with Ru-CeO_2 catalyst, the content of Lewis acid sites on the catalyst

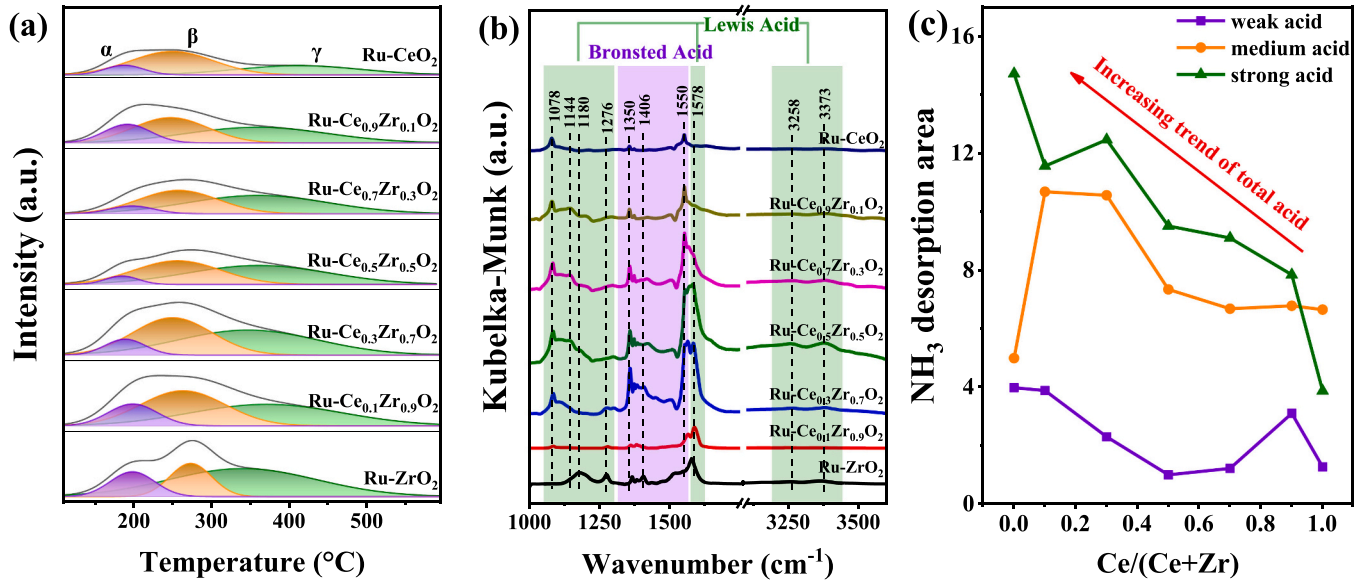

Fig. 4. (a) NH_3-TPD profiles of Ru-$Ce_xZr_{1-x}O_2$ catalysts, (b) in situ DRIFTS of NH_3 adsorption at 100 °C over Ru-$Ce_xZr_{1-x}O_2$ catalysts, (c) change trend of content of weak, medium and strong acid of Ru-$Ce_xZr_{1-x}O_2$ catalysts.

surface greatly increased with formation of the solid solution structure. The adsorption bands at 3258 and 3373 cm^{-1}, ascribed to Lewis acid sites [50], were very weak over Ru-CeO_2 or Ru-ZrO_2 catalysts, but obviously increased over Ru-$Ce_xZr_{1-x}O_2$ catalysts with the solid solution structure. It can be speculated that the solid solution structure is beneficial to produce new Lewis acid sites on the catalyst surface. The adsorption band at 1180 cm^{-1} in Ru-ZrO_2 was assigned to the symmetrical deformation mode in which NH_3, bound on Lewis acid sites, obviously decreased upon Ce doping [46]. According to XRD and Raman results, these Lewis acid sites probably existed on the surface of monoclinic ZrO_2. Lewis acid sites can facilitate adsorption of chlorine species on the catalyst surface in the form of M-Cl bond. The desorption of Cl species is completed by forming highly reactive Cl_2 through Deacon reaction. The formation of M-Cl bond by adsorption of chlorine species on Lewis acid site is a vital step in the catalytic combustion reaction, although Deacon reaction requires a relatively high temperature to occur. As shown in Table S2, the amount of Lewis acids (L-acid amount) of Ru-$Ce_xZr_{1-x}O_2$ catalysts exhibited a volcano trend and Ru-$Ce_{0.5}Zr_{0.5}O_2$ catalyst had the largest L-acid amount. To exclude the effect of S_{BET}, which was related to the elemental ratios in the solid solution structure of the catalysts, the amount of Lewis acids per unit of specific surface area (L-$acid_{pussa}$) of Ru-$Ce_xZr_{1-x}O_2$ catalysts was calculated and shown in Table S2. The L-$acid_{pussa}$ values of Ru-$Ce_xZr_{1-x}O_2$ (x = 0, 0.1, 0.3, 0.5, 0.7, 0.9, 1) catalysts were 0.176, 0.147, 0.121, 0.165, 0.148, 0.161 and 0.147, respectively. The magnitude of L-$acid_{pussa}$ value can reflect the adsorption ability of Ru-$Ce_xZr_{1-x}O_2$ catalyst for chlorine species. In contrast, Brønsted acid can attack M-Cl bond at a relatively low temperature to form HCl, thereby removing the adsorbed chlorine species on Lewis acid sites more rapidly [51]. Therefore, a reasonable distribution of Lewis acid and Brønsted acid is conductive to adsorption and dissociation of VC, and desorption of Cl species on the catalyst surface.

3.5. Reaction mechanism

In situ DRIFTS spectra of co-adsorption of VC and O_2 over Ru-CeO_2, Ru-$Ce_{0.5}Zr_{0.5}O_2$ and Ru-ZrO_2 catalysts are shown in Fig. 5. The bands at 1376–1383 cm^{-1} and 1574–1590 cm^{-1}, assigned to formate moieties, were observed over Ru-$Ce_{0.5}Zr_{0.5}O_2$ (Fig. 5b) and Ru-ZrO_2 (Fig. 5c) catalysts. The bands at ~1547 cm^{-1} and ~1650 cm^{-1}, assigned to acetate moieties, were observed over Ru-CeO_2 (Fig. 5a) and Ru-ZrO_2 catalysts. The bands at 1870 cm^{-1} were attributed to carbonyl moieties over Ru. The main difference lied in the formation of intermediate products among these three catalysts. The first step for VC dissociation is adsorption of Cl on Lewis acid sites, after which the bond energies of C═C and C-Cl bonds get weakened by this chemical adsorption [7]. The weakening of the bond energy enables C-Cl breakage to occur readily, with Cl remaining on the oxygen vacancy and forming M-Cl bond with Lewis acid sites. Meanwhile, the C═C group is converted into a hydrocarbon structure (-C_2H_3) adsorbed on surface oxygen species, and existence of bands at 1180 cm^{-1} assigned to C-O can confirm this process. And the increasing intensity of bands at 1870 cm^{-1} indicates the important role of Ru in further oxidation of hydrocarbon structure. The dissociated Cl species on the oxygen vacancy preferentially react with the surface hydroxyl group (Brønsted acid) and then are desorbed in the form of HCl. The lack of surface acid sites on Ru-CeO_2 catalyst was the main reason for chlorine poisoning. Based on the results of in situ DRIFTS, there were two different oxidation pathways for hydrocarbon intermediates bounded on the catalyst surface, generating formate and acetate species, respectively. Surface chemically adsorbed oxygen species (CAOS), facilitated by Ru-O-Ce structure, could cause a direct cleavage of C-C bond, generating formate species which were more susceptible to further oxidation. However, the amount of CAOS over Ru-CeO_2 catalyst was reduced due to chlorine poisoning and hydrocarbons were then converted to acetate species rather than formate species, which could be confirmed by the differences in change of band intensity between formate moieties and acetate moieties shown in Fig. 5a. In the range of 100–200 °C, the band intensity of acetate moieties significantly enhanced, while that of formate moieties did not obviously change. Over Ru-ZrO_2 catalyst, conversion of hydrocarbons to acetate species and formate species due to enough acid sites avoided chlorine poisoning on the catalyst surface. But the conversion pathway of acetate species dominated due to its lower CAOS amount. The bands at 1430 and 2863 cm^{-1} assigned to methyl or methylene moieties shown in Figs. 5a and 5c, indicated that C-C bond was not broken, which confirmed the reaction pathway for generation of acetate species over Ru-CeO_2 and Ru-ZrO_2 catalysts. As for Ru-$Ce_{0.5}Zr_{0.5}O_2$ catalyst, sufficient Lewis and Brønsted acid sites enabled the timely dissociation and desorption of Cl to avoid chlorine poisoning, while sufficient CAOS promoted cleavage of C-C bonds. Therefore, the easily oxidized formate species were mainly generated during the reaction process, and this was also the reason why Ru-$Ce_{0.5}Zr_{0.5}O_2$ catalyst could exhibit excellent catalytic activity for the catalytic combustion of VC even at high WHSV and VC concentration shown in Figs. 8b and 8c. The carbonyl species were generated by further oxidation of formate and acetate species, which was proved by

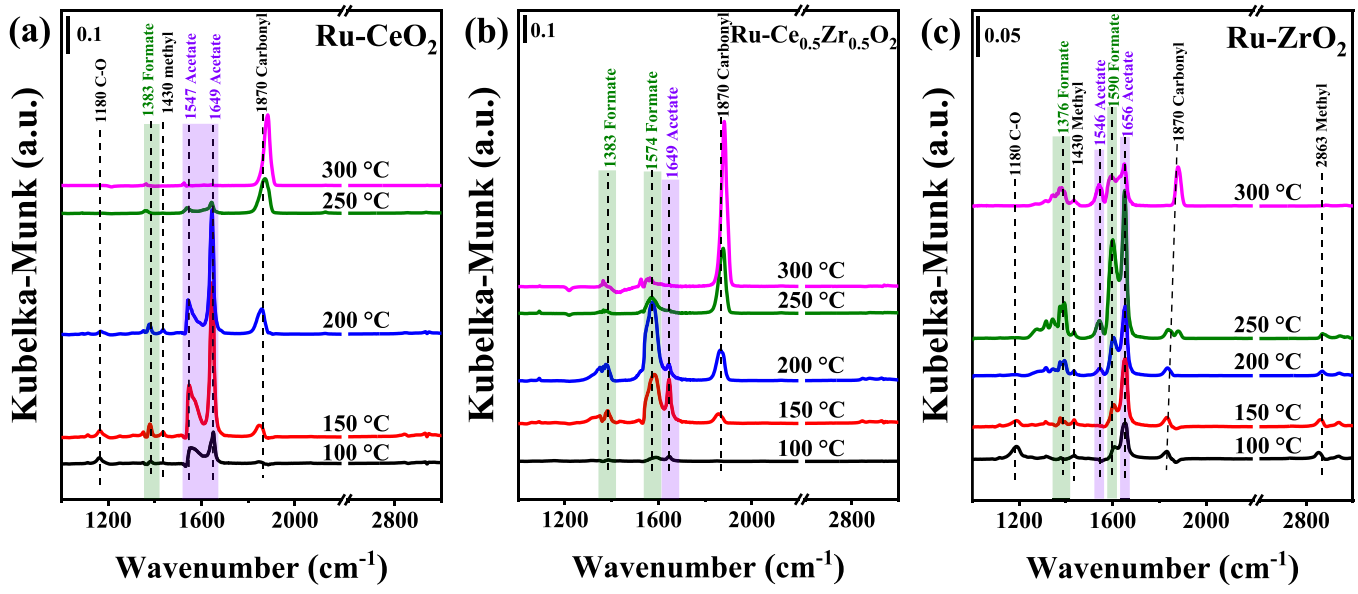

Fig. 5. In situ DRIFTS spectra of co-adsorption of VC and O_2 over Ru-CeO_2 (a), Ru-$Ce_{0.5}Zr_{0.5}O_2$ (b) and Ru-ZrO_2 (c) catalysts.

the weakening of the intensity of formate and acetate bands and the enhancement in the intensity of the carbonyl bands with increasing temperature.

To gain further insights into the reaction process, in situ DRIFTS of VC adsorption, reaction of VC and O_2 at 200 °C over Ru-CeO_2, Ru-$Ce_{0.5}Zr_{0.5}O_2$ and Ru-ZrO_2 catalysts were carried out, and the results are shown in Fig. 6. After adsorption of VC for 30 min, acetate intermediates were mainly observed over Ru-CeO_2 catalyst, while formate intermediates over Ru-$Ce_{0.5}Zr_{0.5}O_2$ catalyst and formate and acetate intermediates over Ru-ZrO_2 catalyst, which was consistent with the results shown in Fig. 5. However, when the feeding gas was changed to VC and O_2, great difference in band intensity of intermediates over these three catalysts happened. As shown in Fig. 6a, there was no obvious change in surface species and the corresponding band intensity over Ru-CeO_2 catalyst after reaction for 30 min, which proved that severe chlorine poisoning occurred on the catalyst surface. As for Ru-$Ce_{0.5}Zr_{0.5}O_2$ catalyst (Fig. 6b), after incorporation of O_2, surface O_v rapidly activated O_2 in the reaction atmosphere, and CAOS was replenished, so the band intensity of formate species was continuously enhanced. Ru-ZrO_2 catalyst (Fig. 6c) benefited from more sufficient acid sites on the catalyst surface to avoid chlorine poisoning during VC adsorption process, so accumulation of all intermediates on the catalyst surface increased during 30 min reaction process, which even exhibited a more obvious enhancement compared with Ru-$Ce_{0.5}Zr_{0.5}O_2$ catalyst. However, the catalytic activity was not solely influenced by the catalyst acidity, and the redox property played a more significant role in the reaction. And obviously, Ru-$Ce_{0.5}Zr_{0.5}O_2$ catalyst exhibited better redox property than Ru-ZrO_2 catalyst according to the above redox results. No observation of acetate species over Ru-$Ce_{0.5}Zr_{0.5}O_2$ catalyst during 30 min experiment also proved that Ru-$Ce_{0.5}Zr_{0.5}O_2$ catalyst exhibited better catalytic activity. Both acetate and formate intermediates were further oxidated to carbonyl over these three catalysts, which was consistent with the results shown in Fig. 5.

Reaction mechanism for catalytic combustion of VC over Ru-CeO_2, Ru-$Ce_{0.5}Zr_{0.5}O_2$ and Ru-ZrO_2 catalysts are proposed in Fig. 7. The amounts of sufficient acid sites and CAOS on the catalyst surface are crucial for efficient catalytic combustion of VC. Ru-CeO_2 catalyst is prone to chlorine poisoning due to lack of sufficient acid sites to desorb Cl species adsorbed on the catalyst surface in a timely manner, which disrupts the rapid cycle of oxygen species on the catalyst surface, hence VC can not be oxidized to easily oxidizable formate species. More acetate species are generated on the surface of Ru-ZrO_2 catalyst due to its poor redox ability. The appropriate amount of Zr doping into Ru-CeO_2 catalyst can simultaneously increase the amounts of acid sites and CAOS, which promotes rapid oxidation of VC and avoids chlorine poisoning on the catalyst surface.

3.6. Catalytic activity, thermal stability and water resistance

The catalytic activity of Ru-$Ce_xZr_{1-x}O_2$ catalysts for the catalytic combustion of VC are shown in Fig. 8a. For Ru-CeO_2 catalyst, T_{50} and T_{90} (the reaction temperature achieved 50% or 90% of VC conversion) were 225 °C and 262 °C, respectively. With doping of Zr into Ru-CeO_2 catalyst, the catalytic activity of Ru-$Ce_xZr_{1-x}O_2$ catalysts with the solid solution structure significantly increased. Additionally, enhancement of the catalytic activity was influenced by the molar ratio of Ce/(Ce + Zr) with a volcano-like trend. Overall, Ru-$Ce_{0.5}Zr_{0.5}O_2$ catalyst showed the best catalytic activity with T_{90} of 227 °C, exhibiting a drop of up to 35 °C compared with Ru-CeO_2 catalyst. To confirm that the optimum molar ratio of Ce/(Ce + Zr) was 0.5, Ru-$Ce_xZr_{1-x}O_2$ catalysts with x = 0.4 and 0.6 were investigated for the catalytic combustion of VC. As shown in Figure S6a, Ru-$Ce_{0.5}Zr_{0.5}O_2$ catalyst also exhibited the best catalytic activity. As shown in Table S3, T_{90} of Ru-$Ce_xZr_{1-x}O_2$ catalysts increased in the following order: Ru-$Ce_{0.5}Zr_{0.5}O_2$ < Ru-$Ce_{0.3}Zr_{0.7}O_2$ < Ru-$Ce_{0.7}Zr_{0.3}O_2$ ≈ Ru-$Ce_{0.9}Zr_{0.1}O_2$ < Ru-$Ce_{0.1}Zr_{0.9}O_2$ < Ru-CeO_2 < Ru-ZrO_2, and Ru-$Ce_{0.5}Zr_{0.5}O_2$ catalyst exhibited the highest reaction rate of 5.48 $*10^{-5}$ $mol \cdot g^{-1} \cdot s^{-1}$.

As shown in Figs. 8b and 8c, even under the reaction conditions of high VC concentration and high WHSV, Ru-$Ce_{0.5}Zr_{0.5}O_2$ catalyst still exhibited superior catalytic activity for the catalytic combustion of VC. When VC concentration increased from 3000 ppm to 9000 ppm and WHSV increased from 60,000 $mL \cdot g^{-1} \cdot h^{-1}$ to 90,000 $mL \cdot g^{-1} \cdot h^{-1}$, there was only a slight decrease in the catalytic activity with a very effective resistance to chlorine poisoning. As shown in Fig. 8d, the catalytic stability of Ru-CeO_2 and Ru-$Ce_{0.5}Zr_{0.5}O_2$ catalysts were investigated by monitoring the change in the catalytic activity of VC combustion at 320 °C (T_{100} for both catalysts), then increased to 500 °C (calcination temperature of the catalysts) and decreased to 320 °C with every temperature lasting for 900 min. Ru-CeO_2 catalyst was rapidly deactivated after reaction at 320 °C for 900 min, in which VC conversion decreased from 100% to 72%. As the reaction temperature increased to 500 °C, VC conversion restored to 100%, but continued to decline to 80% after reaction at 500 °C for another 900 min. When the reaction temperature decreased to 320 °C, VC conversion significantly dropped and remained

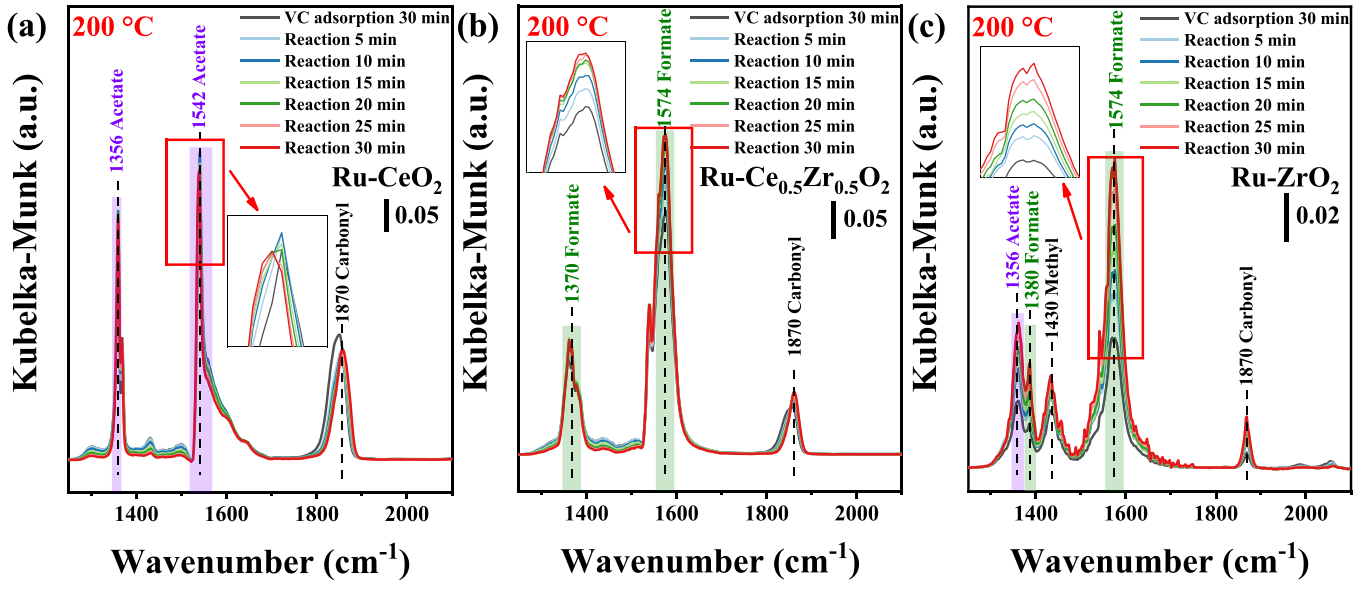

Fig. 6. In situ DRIFTS spectra of VC adsorption, reaction of VC and O_2 at 200 °C over Ru-CeO_2 (a), Ru-$Ce_{0.5}Zr_{0.5}O_2$ (b) and Ru-ZrO_2 (c) catalysts.

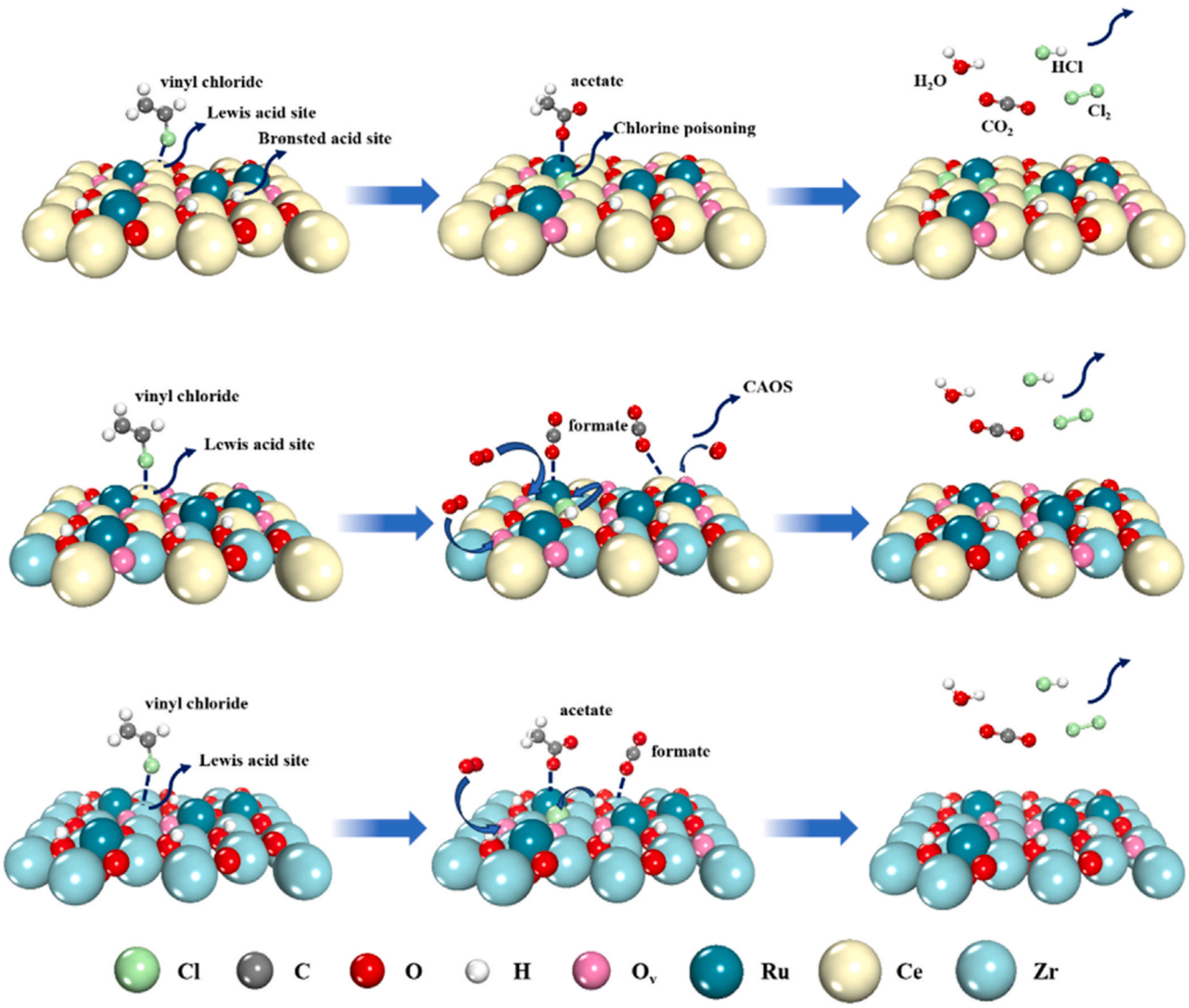

Fig. 7. Reaction mechanism for catalytic combustion of VC over Ru-CeO_2, Ru-$Ce_{0.5}Zr_{0.5}O_2$ and Ru-ZrO_2 catalysts.

at about 33%. The poor catalytic stability of Ru-CeO_2 catalyst was due to chlorine poisoning of the active sites, and an even lower VC conversion in the second stability evaluation at 320 °C indicated that the irreversible structural damage of catalyst happened after the prolonged reaction at 500 °C for 900 min. However, Ru-$Ce_{0.5}Zr_{0.5}O_2$ catalyst maintained VC conversion of 100% throughout the stability evaluation for 2700 min, and no deactivation was observed. The catalytic stability of Ru-ZrO_2 catalyst was also evaluated and shown in Figure S7. Due to the sufficient acid sites on the catalyst surface, which was proved by NH_3-TPD experiment, no obvious deactivation was observed during the evaluation for 2700 min. As shown in Figure S8, even at higher reaction temperature of 650 °C, Ru-$Ce_{0.5}Zr_{0.5}O_2$ catalyst exhibited 100% of VC conversion during the evaluation for 2700 min. Therefore, Ru-$Ce_{0.5}Zr_{0.5}O_2$ catalyst exhibited superior resistance to chlorine poisoning and high catalytic stability.

The main factor affecting the reaction rate of catalyst is the amount of active oxygen species (including CAOS and LOS). According to the above results of the redox ability, Ru-O-Ce structure was quite effective in enhancing the amount of active oxygen species. Therefore, the relationship between content of Ru-O-Ce and content of CAOS and LOS or reaction rate was shown in Fig. 9a. With increasing content of Ru-O-Ce, both content of CAOS and LOS and reaction rate increased as well, proving the enhancement of Ru-O-Ce structure on the redox ability. Moreover, to further determine effects of acid sites and the redox ability on the catalytic activity, the relationship between L-$acid_{pussa}$ or H_2 consumption and T_{90} of Ru-$Ce_xZr_{1-x}O_2$ catalysts were shown in Fig. 9b. Unsurprisingly, among Ru-$Ce_xZr_{1-x}O_2$ catalysts, Ru-$Ce_{0.5}Zr_{0.5}O_2$ catalyst, with the highest amounts of L-$acid_{pussa}$ and H_2 consumption, exhibited the best catalytic activity of T_{90} of 227 °C.

Table S4 compares Ru-$Ce_{0.5}Zr_{0.5}O_2$ catalyst with the reported catalysts for the catalytic combustion of VC. Among all catalysts, Ru-$Ce_{0.5}Zr_{0.5}O_2$ catalyst, with the lowest T_{50} and T_{90}, exhibited the best catalytic activity. The effect of Ru content on the catalytic activity of Ru-$Ce_{0.5}Zr_{0.5}O_2$ catalyst is shown in Figure S6b, in which the catalytic activity increased with increasing Ru content (from 0.1 wt% to 2 wt%). When Ru content was increased to 0.5 wt%, the enhancement of the catalytic activity was not significant with further increasing Ru content. Therefore, 0.5 wt% was chosen as Ru content over the catalysts in this work.

Another problem for the catalytic combustion of CVOCs is the tendency to produce a variety of polychlorinated by-products, causing secondary pollution [52]. As shown in Fig. 10, the polychlorinated by-products were $C_2H_3Cl_3$, CCl_4, $C_2H_4Cl_2$, $C_2H_2Cl_2$, and CH_2Cl_2 over Ru-CeO_2 and Ru-$Ce_{0.5}Zr_{0.5}O_2$ catalysts. The complete combustion

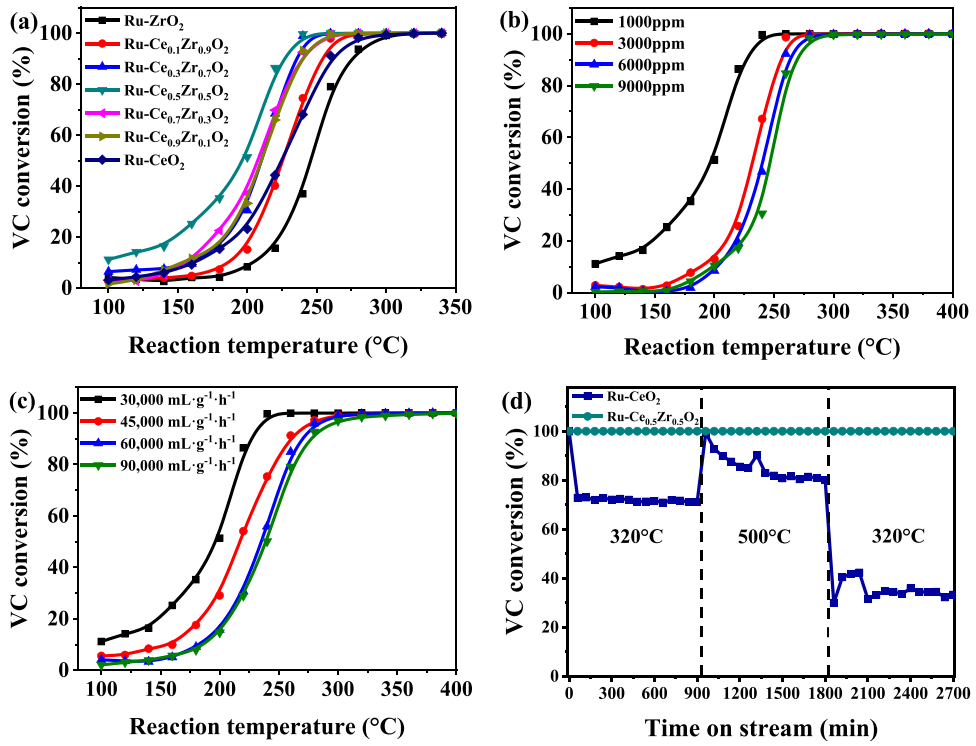

Fig. 8. VC conversion vs. the molar ratio of Ce/(Ce + Zr) (a), VC concentration (b) and WHSV (c) over Ru-$Ce_xZr_{1-x}O_2$ catalysts. Catalytic stability (d) of Ru-CeO_2 and Ru-$Ce_{0.5}Zr_{0.5}O_2$ catalysts. The reaction conditions were 1000 ppm VC and the balanced air, WHSV of 30,000 mL·g^{-1}·h^{-1} for (a), (d).

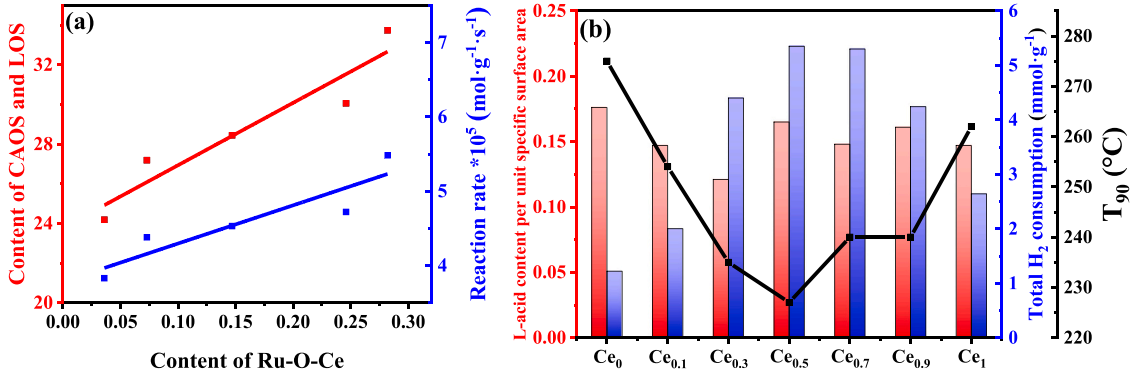

Fig. 9. Change trend of (a) content of CAOS and LOS and reaction rate vs. content of Ru-O-Ce, (b) L-$acid_{pussa}$, H_2 consumption and T_{90} of Ru-$Ce_xZr_{1-x}O_2$ catalysts with different molar ratio of Ce/(Ce+Zr).

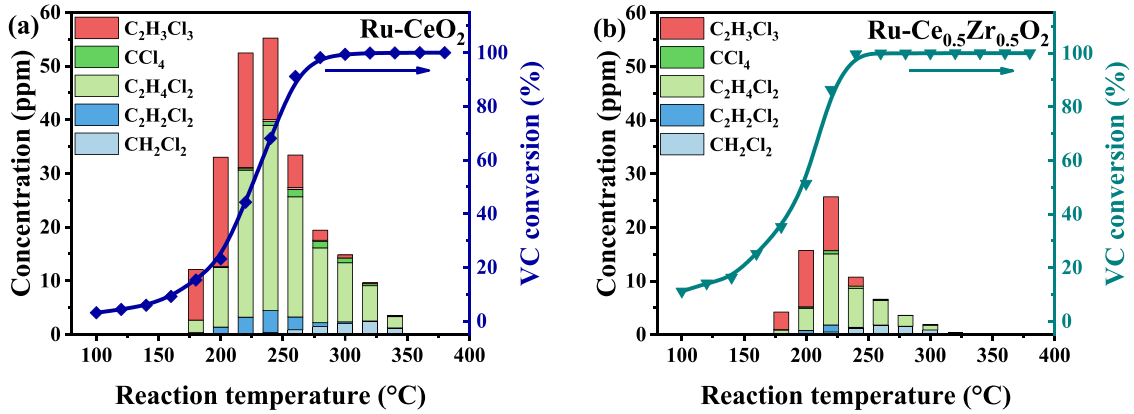

Fig. 10. Concentrations of polychlorinated by-products generated in catalytic combustion of VC over Ru-CeO_2 (a) and Ru-$Ce_{0.5}Zr_{0.5}O_2$ (b) catalysts.

temperature of all by-products was 320 °C over Ru-$Ce_{0.5}Zr_{0.5}O_2$ catalyst and up to 360 °C over Ru-CeO_2 catalyst. Ru-$Ce_{0.5}Zr_{0.5}O_2$ catalyst also showed significantly lower by-product concentration, with the highest total by-product concentration decreasing by more than 50% from ~55 ppm to ~26 ppm, compared with Ru-CeO_2 catalyst. The by-product concentrations over other catalysts are shown in Figure S9. The selectivity of polychlorinated by-products over Ru-$Ce_xZr_{1-x}O_2$ catalysts is shown in Figure S10. The above acidity analysis suggested that Zr doping significantly improve the catalyst acidity. The decrease in the selectivity of polychlorinated by-products with increasing the molar ratio of Zr was due to the enhancement of acidity, which improved the Cl species handling capacity of the catalyst [7]. With increasing the molar ratio of Zr from 0 to 0.5, both the selectivity and the complete combustion temperature of polychlorinated by-products significantly decreased. With further increasing the molar ratio of Zr, although the selectivity of polychlorinated by-products still decreased, the complete combustion temperature of by-products significantly increased due to the poor redox ability. The above by-product results indicated that the appropriate amount of Zr doping into Ru-CeO_2 catalyst was an effective way to enhance the catalytic performance of Ru-$Ce_xZr_{1-x}O_2$ catalyst with less formation of polychlorinated by-products.

5.0 vol% H_2O was injected into the feed gas to investigate the catalytic performance under the near realistic operating conditions. The activity curves, by-product concentrations and catalytic stability with 5.0 vol% water over Ru-$Ce_{0.5}Zr_{0.5}O_2$ and Ru-CeO_2 catalysts are shown in Fig. 11. The catalytic activity with 5.0 vol% water of Ru-$Ce_{0.5}Zr_{0.5}O_2$ catalyst slightly decreased (Fig. 11a) due to the competitive adsorption of H_2O on the active sites of catalyst [18]. Ru-$Ce_{0.5}Zr_{0.5}O_2$ catalyst exhibited better catalytic activity with 5.0 vol% water than Ru-CeO_2 catalyst, with T_{90} increasing from 227 °C to 239 °C, while that of Ru-CeO_2 catalyst increased from 262 °C to 288 °C (Figure S11a). As shown in Figs. 10b and 11b, the by-product concentrations with 5.0 vol % water over Ru-$Ce_{0.5}Zr_{0.5}O_2$ catalyst greatly decreased. The highest by-product concentration at 220 °C, for example, reduced by 52% from ~27 ppm to ~13 ppm. This is because H_2O can provide sufficient surface hydroxyl groups to act as Brønsted acid sites, thus facilitating dissociation of chlorine species adsorbed on the catalyst surface [26]. As shown in Fig. 10a and S11b, for Ru-CeO_2 catalyst, although the by-product concentrations with 5.0 vol% water decreased, the complete combustion temperature of all by-products was increased by 20 °C up to 380 °C.

As shown in Fig. 11c, the catalytic stability was investigated under the reaction condition of injecting 5.0 vol% H_2O for 720 min, and stopping the injection for a continuous 720 min, and then continuing the injection of 5.0 vol% H_2O for another 720 min at the reaction temperature of 320 °C. VC conversion of Ru-CeO_2 catalyst continuously decreased regardless of in presence or absence of H_2O, and the decrease was more obvious in presence of H_2O. However, as shown in Figs. 11c and 8d, the extent of deactivation in presence of H_2O was quite slight, even in the second period in absence of H_2O, indicated that H_2O offered sufficient surface hydroxyl groups to act as Brønsted acid sites to avoid chloride poisoning. For Ru-ZrO_2 catalyst, slight deactivation was observed in presence of H_2O. No deactivation was observed in absence of H_2O due to strong acidity of Ru-ZrO_2 catalyst to avoid chlorine poisoning over the catalyst. As shown in Fig. 11c, for Ru-$Ce_{0.5}Zr_{0.5}O_2$ catalyst, no deactivation was observed in the evaluation of catalytic stability and VC conversion kept 100% within 2160 min. This is because H_2O can continuously replenish Brønsted acid sites consumed on the catalyst surface, which greatly improves the dechlorination efficiency.

In summary, Zr doping effectively improved the catalytic performance of Ru-CeO_2 catalyst, which not only enhanced the catalytic activity of the catalytic combustion of VC, reduced the selectivity and complete combustion temperature of polychlorinated by-products, but also improved the resistance to high temperature, chlorine poisoning and water. In addition, as shown in Figure S12, Ru-$Ce_{0.5}Zr_{0.5}O_2$ catalyst exhibited better catalytic activity for the catalytic combustion of propane, N, N-dimethylformamide (DMF) and dichloroethane (EDC), suggesting that the enhancement of the content of highly reactive Ru-O-Ce structure by formation of the solid solution structure was a generally efficient method to improve the catalytic performance of Ru-$Ce_xZr_{1-x}O_2$ catalyst for the catalytic combustion of various VOCs.

4. Conclusions

Ru-$Ce_xZr_{1-x}O_2$ catalysts were synthesized by stepwise precipitation method and used for the catalytic combustion of VC, in which effect of the molar ratio of Ce/(Ce + Zr) on the physiochemical properties and the catalytic performance of Ru-$Ce_xZr_{1-x}O_2$ catalysts were investigated. It is found that the Ce-O-Zr solid solution structure is generated with Zr doping and greatly increases the defect content on the surface. The solid solution structure enhances SMSI between Ru and Ce thereby increasing the Ru-O-Ce content, which is beneficial to further increase the content of highly reactive CAOS. In addition to the redox ability of Ru-$Ce_xZr_{1-x}O_2$ catalysts, surface acidity is another key factor affecting the catalytic performance, in which Zr doping significantly increases surface acid sites. The different intermediate generation pathways on the catalyst surface and effect of chlorine poisoning over Ru-$Ce_xZr_{1-x}O_2$ catalysts are determined by in situ DRIFTS. Among Ru-$Ce_xZr_{1-x}O_2$ catalysts, Ru-$Ce_{0.5}Zr_{0.5}O_2$ catalyst exhibits the best catalytic performance with T_{90} of 227 °C under the reaction conditions of 1000 ppm VC and WHSV of 30,000 mL·g^{-1}·h^{-1}. Moreover, Ru-$Ce_{0.5}Zr_{0.5}O_2$ catalyst exhibits the superior resistance to high temperature, chlorine poisoning and water, and excellent catalytic activity for the catalytic combustion of various VOCs. This work can provide guidance for designing efficient catalysts for the catalytic combustion of VOCs, and accelerate the development of environmentally friendly catalysts.

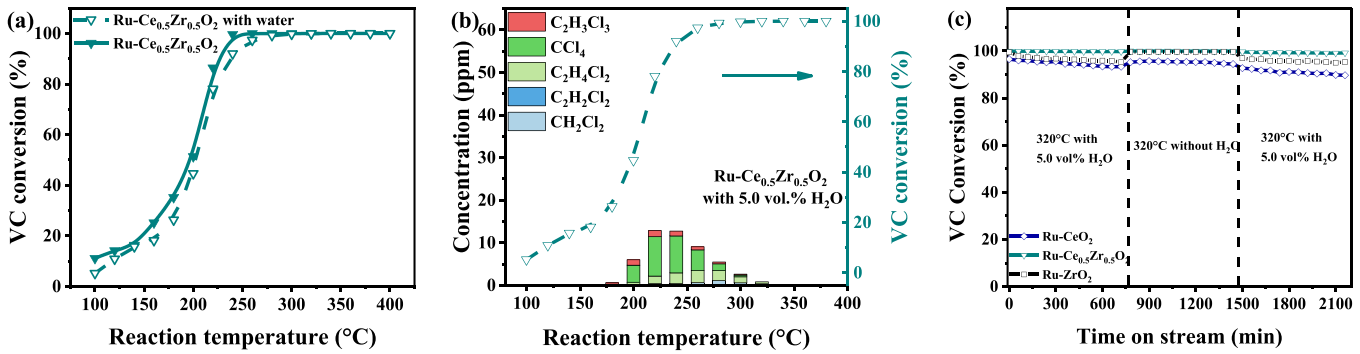

Fig. 11. VC conversion curves (a) and by-product concentrations generated in catalytic combustion of VC (b) with 5.0 vol% water over Ru-$Ce_{0.5}Zr_{0.5}O_2$ catalyst, the catalytic stability at 320 °C with 5.0 vol% water over Ru-CeO_2, Ru-$Ce_{0.5}Zr_{0.5}O_2$ and Ru-ZrO_2 catalysts (c). The reaction conditions were 1000 ppm VC and the balanced air, WHSV of 30,000 mL·g^{-1}·h^{-1}.

CRediT authorship contribution statement

Yanglong Guo: Writing – review & editing, Supervision. **Aiyong Wang:** Writing – original draft, Supervision. **Meixingzi Gao:** Investigation, Data curation. **Min Ding:** Investigation, Data curation. **Zijian Wei:** Methodology, Investigation. **Baocheng Xie:** Writing – original draft, Methodology, Investigation, Data curation, Conceptualization. **Yun Guo:** Resources, Funding acquisition. **Wangcheng Zhan:** Visualization, Validation. **Qiguang Dai:** Visualization, Conceptualization. **Li Wang:** Formal analysis, Conceptualization.

Declaration of Competing Interest

The authors declare that they have no known competing financial interests or personal relationships that could have appeared to influence the work reported in this paper.

Data availability

Data will be made available on request.

Acknowledgements

This work was supported by the National Key Research and Development Program of China (2023YFC3707500, 2022YFB3504200), the National Natural Science Foundation of China (U21A20326, 22106101), the fund of the National Engineering Laboratory for Mobile Source Emission Control Technology (NELMS2020A05), and the Fundamental Research Funds for the Central Universities.

Appendix A. Supporting information

Supplementary data associated with this article can be found in the online version at doi:10.1016/j.apcatb.2024.123926.

References

[1] Y. Su, K.X. Fu, C.H. Pang, Y.F. Zheng, C.F. Song, N. Ji, D.G. Ma, X.B. Lu, C.X. Liu, R. Han, Q.L. Liu, Recent advances of chlorinated volatile organic compounds' oxidation catalyzed by multiple catalysts: reasonable adjustment of acidity and redox properties (https://), Environ. Sci. Technol. 56 (2022) 9854–9871, https://doi.org/10.1021/acs.est.2c01420.

[2] H.Q. Jia, Y. Xing, L.G. Zhang, W.B. Zhang, J.Q. Wang, H. Zhang, W. Su, Progress of catalytic oxidation of typical chlorined volatile organic compounds (CVOCs): a review (https://), Sci. Total Environ. 865 (2023) 161063, https://doi.org/10.1016/j.scitotenv.2022.161063.

[3] H. Zhang, X.H. Gao, B.W. Gong, S.J. Shao, C.S. Tu, J. Pan, Y.Y. Wang, Q.G. Dai, Y. L. Guo, X.Y. Wang, Catalytic combustion of CVOCs over MoO_x/CeO_2 catalysts (https://), Appl. Catal. B: Environ. 310 (2022) 121240, https://doi.org/10.1016/j.apcatb.2022.121240.

[4] L.C. Li, N.Q. Zhang, X. Huang, Y. Liu, Y.Y. Li, G.Z. Zhang, L.Y. Song, H. He, Hydrothermal stability of core–shell $Pd@Ce_{0.5}Zr_{0.5}O_2/Al_2O_3$ catalyst for automobile three-way reaction (https://), ACS Catal. 8 (2018) 3222–3231, https://doi.org/10.1021/acscatal.8b00358.

[5] Z.Y. Li, R.Y. Gao, Z.Q. Hou, X.H. Yu, H.X. Dai, J.G. Deng, Y.X. Liu, Tandem supported Pt and ZSM-5 catalyst with separated catalytic functions for promoting multicomponent VOCs oxidation (https://), Appl. Catal. B: Environ. 339 (2023) 123131, https://doi.org/10.1016/j.apcatb.2023.123131.

[6] P. Yang, S.F. Zuo, R.X. Zhou, Synergistic catalytic effect of $(Ce,Cr)_xO_2$ and HZSM-5 for elimination of chlorinated organic pollutants (https://), Chem. Eng. J. 323 (2017) 160–170, https://doi.org/10.1016/j.cej.2017.04.002.

[7] H. Liu, X. Li, Q.G. Dai, H.L. Zhao, G.T. Chai, Y.L. Guo, Y. Guo, L. Wang, W.C. Zhan, Catalytic oxidation of chlorinated volatile organic compounds over Mn-Ti composite oxides catalysts: elucidating the influence of surface acidity (https://), Appl. Catal. B: Environ. 282 (2021) 119577, https://doi.org/10.1016/j.apcatb.2020.119577.

[8] C. Wang, W.C. Hua, G.T. Chai, C.H. Zhang, Y.L. Guo, Insights into the morphological effect of Co_3O_4 crystallite on catalytic oxidation of vinyl chloride (https://), Catalysts 9 (2019) 408, https://doi.org/10.3390/catal9050408.

[9] Q.G. Dai, X.Y. Wang, G.Z. Lu, Low-temperature catalytic combustion of trichloroethylene over cerium oxide and catalyst deactivation (https://), Appl. Catal. B: Environ. 81 (2008) 192–202, https://doi.org/10.1016/j.apcatb.2007.12.013.

[10] L. Zhang, W. Deng, Y.P. Cai, Q.G. Dai, L.M. Guo, Comparative studies of phosphate-modified CeO_2 and Al_2O_3 for mechanistic understanding of dichloromethane oxidation and chloromethane formation (https://), ACS Catal. 10 (2020) 13109–13124, https://doi.org/10.1021/acscatal.0c02691.

[11] X.L. Liu, L. Chen, T.Y. Zhu, R.L. Ning, Catalytic oxidation of chlorobenzene over noble metals (Pd, Pt, Ru, Rh) and the distributions of polychlorinated by-products (https://), J. Hazard. Mater. 363 (2019) 90–98, https://doi.org/10.1016/j.jhazmat.2018.09.074.

[12] G. Celik, S.A. Ailawar, S. Gunduz, J.T. Miller, P.L. Edmiston, U.S. Ozkan, Aqueous-phase hydrodechlorination of trichloroethylene over Pd-based swellable organically-modified silica (SOMS): Catalyst deactivation due to chloride anions (https://), Appl. Catal. B: Environ. 239 (2018) 654–664, https://doi.org/10.1016/j.apcatb.2018.08.065.

[13] Q.G. Dai, K. Shen, W. Deng, Y.P. Cai, J.R. Yan, J.Y. Wu, L.M. Guo, R. Liu, X. Y. Wang, W.C. Zhan, HCl-Tolerant H_xPO_4/RuO_x-CeO_2 catalysts for extremely efficient catalytic elimination of chlorinated VOCs (https://), Environ. Sci. Technol. 55 (2021) 4007–4016, https://doi.org/10.1021/acs.est.0c08256.

[14] Q.G. Dai, S.X. Bai, Z.Y. Wang, X.Y. Wang, G.Z. Lu, Catalytic combustion of chlorobenzene over Ru-doped ceria catalysts (https://), Appl. Catal. B: Environ. 126 (2012) 64–75, https://doi.org/10.1016/j.apcatb.2012.07.008.

[15] X.L. Weng, P.F. Sun, Y. Long, Q.J. Meng, Z.B. Wu, Catalytic oxidation of chlorobenzene over $Mn_xCe_{1-x}O_2$/HZSM-5 catalysts: a study with practical implications (https://), Environ. Sci. Technol. 51 (2017) 8057–8066, https://doi.org/10.1021/acs.est.6b06585.

[16] Y.P. Long, Q.J. Meng, M.L. Chen, X.Q. Luo, Q.G. Dai, H.F. Lu, Z.B. Wu, X.L. Weng, Selective Ru Adsorption on SnO_2/CeO_2 Mixed oxides for efficient destruction of multicomponent volatile organic compounds: from laboratory to practical possibility (https://), Environ. Sci. Technol. 56 (2022) 9762–9772, https://doi.org/10.1021/acs.est.2c02925.

[17] Q.G. Dai, S.X. Bai, J.W. Wang, M. Li, X.Y. Wang, G.Z. Lu, The effect of TiO_2 doping on catalytic performances of Ru/CeO_2 catalysts during catalytic combustion of chlorobenzene (https://), Appl. Catal. B: Environ. 142 143 (2013) 222–233, https://doi.org/10.1016/j.apcatb.2013.05.026.

[18] W.C. Hua, C.H. Zhang, Y.L. Guo, G.T. Chai, C. Wang, Y. Guo, L. Wang, Y.S. Wang, W.C. Zhan, An efficient $Sn_yMn_{1-y}O_x$ composite oxide catalyst for catalytic combustion of vinyl chloride emissions (https://), Appl. Catal. B: Environ. 255 (2019) 117748, https://doi.org/10.1016/j.apcatb.2019.117748.

[19] P. Kaminski, M. Ziolek, Mobility of gold, copper and cerium species in Au, Cu/Ce, Zr-oxides and its impact on total oxidation of methanol (https://), Appl. Catal. B: Environ. 187 (2016) 328–341, https://doi.org/10.1016/j.apcatb.2016.01.040.

[20] B. de Rivas, C. Sampedro, M. García-Real, R. López-Fonseca, J.I. Gutiérrez-Ortiz, Promoted activity of sulphated Ce/Zr mixed oxides for chlorinated VOC oxidative abatement (https://), Appl. Catal. B: Environ. 129 (2013) 225–235, https://doi.org/10.1016/j.apcatb.2012.09.026.

[21] J.I. Gutiérrez-Ortiz, B. de Rivas, R. López-Fonseca, J.R. González-Velasco, Catalytic purification of waste gases containing VOC mixtures with Ce/Zr solid solutions (https://), Appl. Catal. B: Environ. 65 (2006) 191–200, https://doi.org/10.1016/j.apcatb.2006.02.001.

[22] B. Liu, C.M. Li, G.Q. Zhang, X.S. Yao, S.S.C. Chuang, Z. Li, Oxygen vacancy Promoting dimethyl carbonate synthesis from CO_2 and methanol over Zr-doped CeO_2 nanorods (https://), ACS Catal. 8 (2018) 10446–10456, https://doi.org/10.1021/acscatal.8b00415.

[23] N. Li, C. Descorme, M. Besson, Catalytic wet air oxidation of 2-chlorophenol over Ru loaded $Ce_xZr_{1-x}O_2$ solid solutions (https://), Appl. Catal. B: Environ. 76 (2007) 92–100, https://doi.org/10.1016/j.apcatb.2007.05.013.

[24] S.X. Yang, M. Besson, C. Descorme, Catalytic wet air oxidation of succinic acid over Ru and Pt catalysts supported on $Ce_xZr_{1-x}O_2$ mixed oxides (https://), Appl. Catal. B: Environ. 165 (2015) 1–9, https://doi.org/10.1016/j.apcatb.2014.09.057.

[25] Y.W. Zhang, R. Si, S.J. Li, B.X. Lin, C.H. Yan, Urea-based hydrothermally derived homogeneous nanostructured $Ce_{1-x}Zr_xO_2$ (x = 0-0.8) solid solutions: a strong correlation between oxygen storage ability and lattice strain, J. Phys. Chem. B. 108 (2004) 12481–12488, https://doi.org/10.1021/jp048084b.

[26] S.E. Sivan, K.H. Kang, S.J. Han, O. Francis Ngome Okello, S.-Y. Choi, V. Sudheeshkumar, R.W.J. Scott, H.-J. Chae, S. Park, U.H. Lee, Facile MOF-derived one-pot synthetic approach toward Ru single atoms, nanoclusters, and nanoparticles dispersed on CeO_2 supports for enhanced ammonia synthesis (https://), J. Catal. 408 (2022) 316–328, https://doi.org/10.1016/j.jcat.2022.03.019.

[27] H. Wang, G.Q. Yang, Y.H. Song, Z.T. Liu, Z.W. Liu, Defect-rich $Ce_{1-x}Zr_xO_2$ solid solutions for oxidative dehydrogenation of ethylbenzene with CO_2 (https://), Catal. Today 324 (2019) 39–48, https://doi.org/10.1016/j.cattod.2018.07.051.

[28] Q. Yu, L.J. Liu, L.H. Dong, D. Li, B. Liu, F. Gao, K.Q. Sun, L. Dong, Y. Chen, Effects of Ce/Zr ratio on the reducibility, adsorption and catalytic activity of CuO/$Ce_xZr_{1-x}O_2/\gamma$-Al_2O_3 catalysts for NO reduction by CO (https://), Appl. Catal. B: Environ. 96 (2010) 350–360, https://doi.org/10.1016/j.apcatb.2010.02.032.

[29] H. Huang, Q.G. Dai, X.Y. Wang, Morphology effect of Ru/CeO_2 catalysts for the catalytic combustion of chlorobenzene (https://), Appl. Catal. B: Environ. 158 159 (2014) 96–105, https://doi.org/10.1016/j.apcatb.2014.01.062.

[30] J.Y. Wu, B. Chen, J.R. Yan, X. Zheng, X.Y. Wang, W. Deng, Q.G. Dai, Ultra-active Ru supported on CeO_2 nanosheets for catalytic combustion of Propane: Experimental insights into interfacial active sites (https://), Chem. Eng. J. 438 (2022) 135501, https://doi.org/10.1016/j.cej.2022.135501.

[31] S. Letichevsky, C.A. Tellez, R.Rd Avillez, M.I.Pd Silva, M.A. Fraga, L.G. Appel, Obtaining CeO_2–ZrO_2 mixed oxides by coprecipitation: role of preparation conditions (https://), Appl. Catal. B: Environ. 58 (2005) 203–210, https://doi.org/10.1016/j.apcatb.2004.10.014.

[32] A.L. Chen, Y. Zhou, N. Ta, Y. Li, W.J. Shen, Redox properties and catalytic performance of ceria–zirconia nanorods (https://), Catal. Sci. Technol. 5 (2015) 4184–4192, https://doi.org/10.1039/c5cy00564g.
[33] Y.Q. Ding, Z. Wang, Y.L. Guo, Y. Guo, L. Wang, W.C. Zhan, A novel method for the synthesis of $Ce_xZr_{1-x}O_2$ solid solution with high purity of κappa phase and excellent reactive activity (https://), Catal. Today 327 (2019) 262–270, https://doi.org/10.1016/j.cattod.2018.04.040.
[34] S. Yoon, J. Jo, B. Jeon, J. Lee, M.G. Cho, M.H. Oh, B. Jeong, T.J. Shin, H.Y. Jeong, J.Y. Park, T. Hyeon, K. An, Revealing charge transfer at the interface of spinel oxide and ceria during CO oxidation (https://), ACS Catal. 11 (2021) 1516–1527, https://doi.org/10.1021/acscatal.0c04091.
[35] J. Chen, W.J. Xu, M.Z. Jiang, J. Chen, H.P. Jia, Polyoxometallate functionalizing CeO_2 via redox-etching precipitation to synergistically catalyze oxidation of gaseous chlorinated pollutants: from lab to practice (https://), Appl. Catal. B: Environ. 278 (2020) 119263, https://doi.org/10.1016/j.apcatb.2020.119263.
[36] Y. Huang, M.J. Tian, Z.Y. Jiang, M.D. Ma, C.W. Chen, H. Xu, J.J. Zhang, R. Albilali, C. He, Inserting Cr_2O_3 dramatically promotes RuO_2/TiO_2 catalyst for low-temperature 1,2-dichloroethane deep destruction: Catalytic performance and synergy mechanism (https://), Appl. Catal. B: Environ. 304 (2022) 121002, https://doi.org/10.1016/j.apcatb.2021.121002.
[37] S. Lee, H. Han, W. Yoon, W.B. Kim, Catalytic complete oxidation of 1,2-dichloroethane over Al-Ti mixed oxide supported VO_x catalyst (https://), Appl. Catal. A: Gen. 611 (2021) 117970, https://doi.org/10.1016/j.apcata.2020.117970.
[38] D.J. Morgan, Resolving ruthenium: XPS studies of common ruthenium materials (https://), Surf. Interface Anal. 47 (2015) 1072–1079, https://doi.org/10.1002/sia.5852.
[39] O. Khalid, T. Weber, G. Drazic, I. Djerdj, H. Over, Mixed $Ru_xIr_{1-x}O_2$ oxide catalyst with well-defined and varying composition applied to CO (https://), Oxid., J. Phys. Chem. C. 124 (2020) 18670–18683, https://doi.org/10.1021/acs.jpcc.0c06392.
[40] Z. Wang, O. Khalid, W. Wang, Y. Wang, T. Weber, A. Spriewald Luciano, W. Zhan, B.M. Smarsly, H. Over, Comparison study of the effect of CeO_2-based carrier materials on the total oxidation of CO, methane, and propane over RuO_2 (https://), Catal. Sci. Technol. 11 (2021) 6839–6853, https://doi.org/10.1039/d1cy01277k.
[41] J.H. Li, Z.Q. Liu, D.A. Cullen, W.H. Hu, J.E. Huang, L.B. Yao, Z.M. Peng, P.L. Liao, R.G. Wang, Distribution and valence state of Ru species on CeO_2 supports: support shape effect and its influence on CO oxidation (https://), ACS Catal. 9 (2019) 11088–11103, https://doi.org/10.1021/acscatal.9b03113.
[42] Y. Guo, S. Mei, K. Yuan, D.J. Wang, H.C. Liu, C.H. Yan, Y.W. Zhang, Low-temperature CO_2 methanation over CeO_2-supported Ru single atoms, nanoclusters, and nanoparticles competitively tuned by strong metal–support interactions and H-spillover effect (https://), ACS Catal. 8 (2018) 6203–6215, https://doi.org/10.1021/acscatal.7b04469.
[43] J. Okal, M. Zawadzki, P. Kraszkiewicz, K. Adamska, Ru/CeO_2 catalysts for combustion of mixture of light hydrocarbons: effect of preparation method and metal salt precursors (https://), Appl. Catal. A: Gen. 549 (2018) 161–169, https://doi.org/10.1016/j.apcata.2017.09.036.
[44] Z.W. Ma, S.L. Zhao, X.P. Pei, X.M. Xiong, B. Hu, New insights into the support morphology-dependent ammonia synthesis activity of Ru/CeO_2 catalysts (https://), Catal. Sci. Technol. 7 (2017) 191–199, https://doi.org/10.1039/c6cy02089e.
[45] F. Wang, C.M. Li, X.Y. Zhang, M. Wei, D.G. Evans, X. Duan, Catalytic behavior of supported Ru nanoparticles on the {1 0 0}, {1 1 0}, and {1 1 1} facet of CeO_2 (https://), J. Catal. 329 (2015) 177–186, https://doi.org/10.1016/j.jcat.2015.05.014.
[46] T. Cai, H. Huang, W. Deng, Q.G. Dai, W. Liu, X.Y. Wang, Catalytic combustion of 1,2-dichlorobenzene at low temperature over Mn-modified Co_3O_4 catalysts (https://), Appl. Catal. B: Environ. 166 167 (2015) 393–405, https://doi.org/10.1016/j.apcatb.2014.10.047.
[47] Y. Kuwahara, Y. Magatani, H. Yamashita, Ru nanoparticles confined in Zr-containing spherical mesoporous silica containers for hydrogenation of levulinic acid and its esters into γ-valerolactone at ambient conditions (https://), Catal. Today 258 (2015) 262–269, https://doi.org/10.1016/j.cattod.2015.01.015.
[48] Y.P. Zhang, W.Q. Guo, L.F. Wang, M. Song, L.J. Yang, K. Shen, H.T. Xu, C.C. Zhou, Characterization and activity of V_2O_5-CeO_2/TiO_2-ZrO_2 catalysts for NH_3-selective catalytic reduction of NOx (https://), Chin. J. Catal. 36 (2015) 1701–1710, https://doi.org/10.1016/s1872-2067(14)60916-0.
[49] B.L. Zhang, S.G. Zhang, B. Liu, H.L. Shen, L. Li, High N_2 selectivity in selective catalytic reduction of NO with NH_3 over Mn/Ti-Zr catalysts (https://), RSC Adv. 8 (2018) 12733–12741, https://doi.org/10.1039/c8ra00336j.
[50] Z.B. Xiong, X.K. Qu, Y.P. Du, C.X. Li, J. Liu, W. Lu, S.M. Wu, Selective catalytic reduction of NO_x with NH_3 over cerium–tungsten–titanium mixed oxide catalyst: Synergistic promotional effect of H_2O_2 and Ce^{4+} (https://), J. Mater. Res. 35 (2020) 2218–2229, https://doi.org/10.1557/jmr.2020.203.
[51] X.L. Lv, S.C. Cai, J. Chen, D.X. Yan, M.Z. Jiang, J. Chen, H.P. Jia, Tuning the degradation activity and pathways of chlorinated organic pollutants over CeO_2 catalyst with acid sites: synergistic effect of Lewis and Brønsted acid sites (https://), Catal. Sci. Technol. 11 (2021) 4581–4595, https://doi.org/10.1039/d1cy00626f.
[52] K. Shen, B. Gao, H.Q. Xia, W. Deng, J.R. Yan, X.H. Guo, Y.L. Guo, X.Y. Wang, W. C. Zhan, Q.G. Dai, Oxy-anionic doping: a new strategy for improving selectivity of Ru/CeO_2 with synergetic versatility and thermal stability for catalytic oxidation of chlorinated volatile organic compounds (https://), Environ. Sci. Technol. 56 (2022) 8854–8863, https://doi.org/10.1021/acs.est.2c00942.